CrossMark

The generation and diffusion of vorticity in three-dimensional flows: Lyman's flux

S.J. Terrington[1],†, K. Hourigan[1] and M.C. Thompson[1]

[1]Fluids Laboratory for Aeronautical and Industrial Research (FLAIR), Department of Mechanical and Aerospace Engineering, Monash University, Melbourne, VIC 3800, Australia

We examine Lyman's (*Appl. Mech. Rev.*, vol. 43, issue 8, 1990, pp. 157–158) proposed definition of the boundary vorticity flux, as an alternative to the traditional definition provided by Lighthill (Introduction: boundary layer theory. In *Laminar Boundary Layers* (ed. L. Rosenhead), chap. 2, 1963, pp. 46–109. Oxford University Press). While either definition may be used to describe the generation and diffusion of vorticity, Lyman's definition offers several conceptual benefits. First, Lyman's definition can be interpreted as the transfer of circulation across a boundary, due to the acceleration of that boundary, and is therefore closely tied to the dynamics of linear momentum. Second, Lyman's definition allows the vorticity creation process on a solid boundary to be considered essentially inviscid, effectively extending Morton's (*Geophys. Astrophys. Fluid Dyn.*, vol. 28, 1984, pp. 277–308) two-dimensional description to three-dimensional flows. Third, Lyman's definition describes the fluxes of circulation acting in any two-dimensional reference surface, enabling a control-surface analysis of three-dimensional vortical flows. Finally, Lyman's definition more clearly illustrates how the kinematic condition that vortex lines do not end in the fluid is maintained, providing an elegant description of viscous processes such as vortex reconnection. The flow over a sphere, in either translational or rotational motion, is examined using Lyman's definition of the vorticity flux, demonstrating the benefits of the proposed framework in understanding the dynamics of vortical flows.

Key words: vortex dynamics

1. Introduction

Vorticity has long been recognised as one of the most important quantities in fluid mechanics. Defined mathematically as the curl of the velocity field,

$$\boldsymbol{\omega} = \nabla \times \boldsymbol{u}, \tag{1.1}$$

† Email address for correspondence: stephen.terrington@monash.edu

vorticity has a clear physical interpretation as twice the mean rotation rate of material lines within a fluid element, or equivalently as twice the local angular velocity of a fluid element (Truesdell 1954). A wide range of important flow phenomena, including boundary layers, wakes and turbulence, can be identified as coherent structures in the vorticity field. Indeed, vortical structures are of such significance that they are considered the 'sinews and muscles of fluid motions' (Küchemann 1965). In light of this, the study of fluid flows in terms of vorticity often provides a deeper understanding of flow behaviour than momentum considerations alone (Lighthill 1963).

A transport equation for vorticity – the Helmholtz vorticity equation – is obtained by taking the curl of the Navier–Stokes equations. For an incompressible, Newtonian fluid, this equation may be expressed as

$$\frac{\partial \boldsymbol{\omega}}{\partial t} + \boldsymbol{u} \cdot \nabla \boldsymbol{\omega} = \boldsymbol{\omega} \cdot \nabla \boldsymbol{u} + \nu \nabla^2 \boldsymbol{\omega}. \tag{1.2}$$

The left-hand side of this equation is the material derivative of vorticity, while the first term on the right-hand side represents the effects of vortex stretching and tilting. The final term is related to the viscous diffusion of linear momentum (Lighthill 1963; Morton 1984), and is usually interpreted as representing the viscous diffusion of vorticity.

Despite being a well-defined mathematical quantity with clear physical significance, and which obeys a known differential equation, the behaviour of vorticity near boundaries has been controversial. This is of particular concern since boundaries are the source of all vorticity in incompressible flows (Morton 1984).

For solid boundaries, Lighthill (1963) defined the boundary vorticity flux,

$$\boldsymbol{\sigma}' = -\nu \hat{\boldsymbol{n}} \cdot \nabla \boldsymbol{\omega}, \tag{1.3}$$

as the rate at which vorticity is created on a section of solid boundary (Lighthill's original definition was for a plane surface; the specific form in (1.3) was first given by Panton 1984). Note that in (1.3), $\hat{\boldsymbol{n}}$ is the unit normal directed into the fluid (i.e. out of the solid boundary). Lyman (1990), however, has proposed an alternative definition of the boundary vorticity flux,

$$\boldsymbol{\sigma} = \nu \hat{\boldsymbol{n}} \times (\nabla \times \boldsymbol{\omega}), \tag{1.4}$$

which provides a different measure of the local vorticity creation rate. Importantly, both definitions return the viscous term in (1.2), $\nu \nabla^2 \boldsymbol{\omega}$, when integrated across a closed surface (see § 1.1), and therefore both describe the correct kinematic evolution of the vorticity field. Perhaps unexpectedly, the dynamical interpretation of the motion provided by each definition differs, and it is currently unclear which definition should be used.

One of the main advantages of Lyman's definition is that it allows Morton's (1984) inviscid description of vorticity creation to be directly applied to three-dimensional flows (Lyman 1990). Lyman's flux is equal to the tangential viscous acceleration of boundary fluid elements and may be substituted for the viscous term in the momentum equation. This yields the following expression for the vorticity creation rate on a no-slip boundary (Lyman 1990; Eyink 2008):

$$\boldsymbol{\sigma} = -\hat{\boldsymbol{n}} \times \left[\frac{\mathrm{d}\boldsymbol{u}}{\mathrm{d}t} + \nabla \left(\frac{p}{\rho} \right) \right]. \tag{1.5}$$

Morton (1984) provides the following interpretation: terms on the right-hand side represent the generation of circulation on the boundary due to the relative acceleration between fluid elements and the boundary, driven by either tangential acceleration of the

boundary or tangential pressure gradients along the boundary. Under this interpretation, viscous forces are not directly responsible for the generation of vorticity, but drive the diffusion of vorticity away from the wall once it has been generated. This inviscid mechanism is considered in more detail in § 3.

Under Lighthill's definition, the boundary flux is not equal to the tangential viscous acceleration, except in two-dimensions, and an additional viscous term must be included in the momentum equation (Wu & Wu 1993):

$$\boldsymbol{\sigma}' = -\hat{\boldsymbol{n}} \times \left[\frac{\mathrm{d}\boldsymbol{u}}{\mathrm{d}t} + \boldsymbol{\nabla} \left(\frac{p}{\rho} \right) \right] - \nu \boldsymbol{\nabla} \boldsymbol{\omega} \cdot \hat{\boldsymbol{n}}. \tag{1.6}$$

Morton's interpretation does not apply when using Lighthill's definition of the vorticity flux, and it is not easy to attach a distinct physical meaning to the viscous term.

There has been some disagreement as to whether Lyman's proposal is appropriate. In particular, Wu & Wu (1993, 1996, 1998) assert that Lyman's proposal is not correct and that Lighthill's original definition must be used. On the other hand, Kolár (2003) appears to accept that either definition may be used, while Eyink (2008) and Eyink, Gupta & Zaki (2020) prefer Lyman's definition. It remains unclear, then, whether it is appropriate to use Lyman's definition of the boundary vorticity flux.

Our interest in Lyman's flux is motivated by a conservation-law formulation of vorticity generation in two-dimensional flows (Terrington, Hourigan & Thompson 2020). We have shown that Morton's inviscid description can be applied not only to solid boundaries, but also to free-surfaces and generalised interfaces, and that this approach leads to an expression of the conservation of global circulation. Lyman's definition of the vorticity flux more readily affords an extension of this formulation to three-dimensional flows, and hence we are compelled to revisit Lyman's proposition, to determine whether it is appropriate and what extra value it provides.

While Wu & Wu (1993, 1996, 1998) insist that only one definition of the vorticity flux can give the 'actual' rate of vorticity creation, Lyman (1990) is comfortable with the notion that there can be more than one way to define the vorticity flux. This ambiguity is discussed in § 1.1, where, in agreement with Lyman, we argue that either definition may be used. The main focus of the present article is not to determine which of two competing definitions is correct, but to illustrate how Lyman's flux enables a clearer and more insightful description of vorticity dynamics.

In addition to extending Morton's (1984) description of vorticity creation to three-dimensional flows, we find the following advantages to using Lyman's definition of the vorticity flux. First, Lyman's definition relates the transfer of circulation between adjacent fluid volumes to the tangential acceleration of fluid on the boundary between these volumes, clearly illustrating the kinematic relationship between vorticity and velocity (§ 1.2). Second, Lyman's flux describes the transfer of circulation (normal vorticity) along any two-dimensional reference surface, so that many aspects of three-dimensional flows can be understood by considering the fluxes of vorticity in a suitable reference surface. Finally, Lyman's flux clearly illustrates how the kinematic property that vortex lines do not end inside a fluid domain (except at null points) is maintained. In viscous vortex connection (§ 2.3), for example, the same terms in Lyman's flux govern the rate of both cutting and reconnection of vortex lines, thereby ensuring that vortex lines do not end inside the fluid.

The structure of this article is as follows. A review of some theoretical aspects in regards to Lighthill's and Lyman's flux definitions is provided in §§ 1.1 and 1.2. In § 2, we present an interpretation of the diffusion of vorticity in the interior of a fluid domain, under

Lyman's flux. In §3, we discuss the generation of vorticity on solid boundaries under Lyman's definition, based on Morton's (1984) inviscid theory. Finally, in §4, various aspects of the formulation are highlighted by the analysis of flow over spheres, in either translational or rotational motion.

1.1. *The uniqueness of the vorticity flux*

In this section, we consider the ambiguity in the definition of the vorticity flux introduced by Lyman (1990), and suggest that either definition may be used. Lighthill's original definition of the boundary vorticity flux ((1.3)) was defined by an analogy with the heat flux in Fourier's law, and may be justified by integration of the viscous term in Helmholtz' equation ((1.2)), across a control volume, V,

$$\int_V \nu \nabla^2 \boldsymbol{\omega} \, \mathrm{d}V = \oint_{\partial V} \nu \hat{\boldsymbol{n}} \cdot \nabla \boldsymbol{\omega} \, \mathrm{d}S, \tag{1.7}$$

where $\hat{\boldsymbol{n}}$ is now the outward-oriented unit normal vector. The integral of $\boldsymbol{\sigma}'$ across a closed boundary, ∂V, is equal to the rate of change of total vorticity in V, so that $\boldsymbol{\sigma}'$ can be considered the local rate of transport of vorticity per unit area across ∂V. Lighthill's definition is not unique, however, and Lyman's (1990) definition ((1.4)) is obtained by using the following equivalent form of the viscous diffusion term:

$$\int_V \nu \nabla^2 \boldsymbol{\omega} \, \mathrm{d}V = \int_V -\nu \nabla \times (\nabla \times \boldsymbol{\omega}) \, \mathrm{d}V = -\oint_{\partial V} \nu \hat{\boldsymbol{n}} \times (\nabla \times \boldsymbol{\omega}) \, \mathrm{d}S. \tag{1.8}$$

While both $\boldsymbol{\sigma}$ and $\boldsymbol{\sigma}'$ may be interpreted as the local flux of vorticity across ∂V, each definition gives different local contributions in three-dimensional flows. In particular, each definition provides a different measure of the local vorticity creation rate on a section of solid boundary. However, both definitions yield the same change in vorticity within any closed fluid volume, and both give the correct evolution of the vorticity field – only the dynamical interpretation of the motion differs between the definitions.

It should be stressed that while both Lighthill (1963) and Lyman (1990) only define the boundary vorticity flux at a solid boundary, the surface ∂V in (1.7) and (1.8) may refer to either the boundary of a fluid domain or of an arbitrary control volume in the fluid interior. In this sense, both Lyman's and Lighthill's definitions may be extended to the transport of vorticity in the fluid interior. In this article, vorticity fluxes are applied to the diffusion of vorticity in the fluid interior, in addition to the creation of vorticity on solid boundaries.

It may be possible to justify a particular definition of the vorticity flux by invoking physical arguments. In the momentum equation, for example, the stress tensor, $\boldsymbol{T} = \mu[\nabla \boldsymbol{u} + (\nabla \boldsymbol{u})^{\mathrm{T}}]$, plays a similar role to the vorticity flux tensor ((1.13)). While an alternative stress tensor, $\boldsymbol{T}' = \mu \nabla \boldsymbol{u}$, would produce the same viscous term in the momentum equation, $\boldsymbol{T}'$ may be rejected on physical grounds, as only $\boldsymbol{T}$ corresponds to the physical force acting on the boundary (Gresho 1991). It is unclear, however, what physical principle could differentiate between $\boldsymbol{\sigma}$ and $\boldsymbol{\sigma}'$. The boundary vorticity flux is deduced from the mathematical structure of the Helmholtz equation, rather than by physical considerations, leaving no obvious reason to prefer either definition.

If momentum and pressure are taken to be the primary variables of fluid mechanics, the diffusion of vorticity occurs as a consequence of the diffusion of linear momentum (Lighthill 1963; Morton 1984), owing to the kinematic relationship between velocity and vorticity. It is often convenient, however, to treat vorticity as the primary variable, and viscous diffusion as a process which distributes vorticity throughout the fluid.

Both definitions of the vorticity flux provide alternative interpretations of this process; however, there is no obvious physical justification to prefer either definition. Wu & Wu (1993, 1996) argue that Lyman's proposed definition is not appropriate, and $\boldsymbol{\sigma}'$ is the only correct measure of the vorticity creation rate. The right-hand side of (1.4) is the tangential viscous acceleration of a boundary fluid element, which includes contributions to the net viscous force applied to a fluid element by both the boundary, and the fluid interior. Since Lyman's definition does not represent a process occurring solely on the solid boundary, Wu & Wu argue that it cannot describe a vorticity creation process occurring on that boundary. However, both $\boldsymbol{\sigma}$ and $\boldsymbol{\sigma}'$ are related to gradients in the shear-stress, so neither can represent the sole action of the boundary on boundary fluid elements. If Lyman's definition is to be rejected on this basis, Lighthill's definition must also be rejected.

1.2. *Kinematics of vorticity transport*

In this section, the vorticity flux is discussed in regard to the kinematic relationship between velocity and vorticity. By using the following vector identity, the volume integral of vorticity can be expressed in terms of the tangential velocity on the boundary:

$$\boldsymbol{\Gamma} = \int_V \boldsymbol{\omega}\,\mathrm{d}V = \oint_{\partial V} \hat{\boldsymbol{n}} \times \boldsymbol{u}\,\mathrm{d}S, \tag{1.9}$$

where $\boldsymbol{\Gamma}$ shall be named the 'vector circulation'. For a stationary control volume, the rate of change of vector circulation depends on the tangential acceleration on the boundary,

$$\int_V \frac{\partial \boldsymbol{\omega}}{\partial t}\,\mathrm{d}V = \oint_{\partial V} \hat{\boldsymbol{n}} \times \frac{\partial \boldsymbol{u}}{\partial t}\,\mathrm{d}S = \oint_{\partial V} \hat{\boldsymbol{n}} \times \left[\boldsymbol{u} \times \boldsymbol{\omega} - \nu \boldsymbol{\nabla} \times \boldsymbol{\omega} - \boldsymbol{\nabla}\left(\frac{p}{\rho} + \frac{1}{2}\boldsymbol{u}\cdot\boldsymbol{u}\right)\right]\mathrm{d}S, \tag{1.10}$$

which is expressed as advection, pressure and viscous terms through the momentum equation. The viscous term, $-\nu\hat{\boldsymbol{n}} \times (\boldsymbol{\nabla} \times \boldsymbol{\omega})$, is Lyman's flux, providing the following physical interpretation: Lyman's flux represents a transfer of circulation between adjacent fluid volumes by the tangential viscous acceleration of fluid on the boundary between the two volumes.

A similar argument, based on Kelvin's circulation theorem, has been presented by Kolár (2003) and Eyink (2008). The rate of change of circulation contained in a closed material curve, C, is given by

$$\frac{\mathrm{d}}{\mathrm{d}t}\int_S \boldsymbol{\omega}\cdot\mathrm{d}\boldsymbol{S} = \frac{\mathrm{d}}{\mathrm{d}t}\oint_C \boldsymbol{u}\cdot\mathrm{d}\boldsymbol{s} = -\oint_C \left(\nu\hat{\boldsymbol{n}} \times (\boldsymbol{\nabla} \times \boldsymbol{\omega})\right)\cdot\hat{\boldsymbol{s}}\,\mathrm{d}s, \tag{1.11}$$

where $\hat{\boldsymbol{s}}$ is the unit normal to S, and $\hat{\boldsymbol{n}}$ is normal to C, but tangent to S, as illustrated in figure 1 (see Kolár (2003) for details). The integrand in (1.11) is the component of Lyman's flux which describes the flux of $\hat{s}$-oriented vorticity in the $\hat{n}$ direction, and represents the rate of change of circulation in C due to the tangential viscous acceleration of a section of boundary.

Wu & Wu (1998) present a variant of (1.11) that supports Lighthill's original definition, rather than Lyman's. However, in their derivation, they neglect a term related to the curvature of vortex lines, on the basis that C may be made arbitrarily small, so that the curvature of C is always much greater than the curvature of vortex lines. However, the curvature of C does not appear in their expression, so the vortex-line curvature term cannot be neglected on this basis. If the curvature term is not neglected, Lyman's definition, rather than Lighthill's, is obtained.
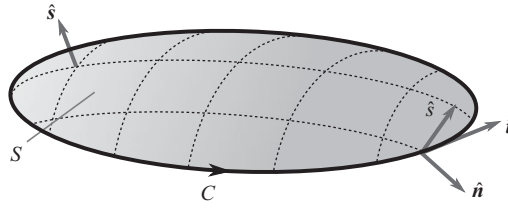
Figure 1. Material surface, S, with boundary curve, C. $\hat{s}$ is the unit normal to S, $\hat{n}$ is a unit normal to C, which lies in the tangent plane of S, and $\hat{t}$ is the unit tangent vector to C.

While the boundary vorticity flux is defined only at the boundary of a fluid domain, it is possible to define a 'vorticity flux tensor', applicable to the diffusion of vorticity in the fluid interior. The differential form of (1.10) is obtained by taking the curl of the Navier–Stokes equations, giving

$$\frac{\partial \boldsymbol{\omega}}{\partial t} = -\boldsymbol{\nabla} \times [-\boldsymbol{u} \times \boldsymbol{\omega} + \nu \boldsymbol{\nabla} \times \boldsymbol{\omega}] = -\boldsymbol{\nabla} \times \boldsymbol{j}. \tag{1.12}$$

This can also be expressed as the divergence of a vorticity flux tensor (Huggins 1971, 1994; Huggins & Bacon 1980; Kolár 2003),

$$\frac{\partial \boldsymbol{\omega}}{\partial t} = -\boldsymbol{\nabla} \cdot \left[\boldsymbol{u}\boldsymbol{\omega} - \boldsymbol{\omega}\boldsymbol{u} - \nu \left(\boldsymbol{\nabla}\boldsymbol{\omega} - (\boldsymbol{\nabla}\boldsymbol{\omega})^{\mathrm{T}} \right) \right] = -\boldsymbol{\nabla} \cdot \boldsymbol{J}. \tag{1.13}$$

The vorticity flux tensor, $\boldsymbol{J}$, is an antisymmetric tensor, with a corresponding axial vector, $\hat{\boldsymbol{j}}$, defined in (1.12). The flux tensor is interpreted as follows: $\hat{\boldsymbol{n}} \cdot \boldsymbol{J} \cdot \hat{\boldsymbol{b}} = (\hat{\boldsymbol{n}} \times \boldsymbol{j}) \cdot \hat{\boldsymbol{b}}$ represents the rate at which the component of vorticity aligned with $\hat{\boldsymbol{b}}$ is transported in the $\hat{\boldsymbol{n}}$ direction, by advection, tilting and viscous diffusion.

Both $\boldsymbol{J}$ and $\boldsymbol{j}$ are closely related to Lyman's definition of the boundary vorticity flux. The flux of vorticity in the $\hat{\boldsymbol{n}}$ direction is given by

$$\hat{\boldsymbol{n}} \cdot \boldsymbol{J} = \hat{\boldsymbol{n}} \times \boldsymbol{j} = -\hat{\boldsymbol{n}} \times (\boldsymbol{u} \times \boldsymbol{\omega}) + \nu \hat{\boldsymbol{n}} \times (\boldsymbol{\nabla} \times \boldsymbol{\omega}), \tag{1.14}$$

and includes a term closely related to Lyman's definition. In particular, if $\hat{\boldsymbol{n}}$ is the unit normal to a solid boundary, then the viscous term in (1.14) is precisely Lyman's definition of the boundary vorticity flux, $\boldsymbol{\sigma}$. Therefore, $\boldsymbol{J}$, and its dual-vector representation, $\hat{\boldsymbol{j}}$, can be understood as a generalisation of Lyman's definition of the boundary vorticity flux to the transport of vorticity in the fluid interior. The antisymmetric tensor, $\boldsymbol{J}$, was first used by Huggins (1971, 1994) to describe vorticity transport in the fluid interior, so shall be referred to in this article as the Lyman–Huggins flux tensor. Similarly, $\hat{\boldsymbol{j}}$ shall be termed the Lyman–Huggins axial flux vector.

The term $(\boldsymbol{\nabla}\boldsymbol{\omega})^{\mathrm{T}}$ in (1.13) is divergence-free and therefore has no effect on $\partial \boldsymbol{\omega}/\partial t$. The 'effective' flux tensor (Kolár 2003),

$$\boldsymbol{J}' = \boldsymbol{u}\boldsymbol{\omega} - \boldsymbol{\omega}\boldsymbol{u} - \nu \boldsymbol{\nabla}\boldsymbol{\omega}, \tag{1.15}$$

considers only the terms which produce a change in the local vorticity. $\boldsymbol{J}'$ generalises Lighthill's definition of the boundary vorticity flux,

$$\hat{\boldsymbol{n}} \cdot \boldsymbol{J}' = -\hat{\boldsymbol{n}} \times (\boldsymbol{u} \times \boldsymbol{\omega}) - \nu \hat{\boldsymbol{n}} \cdot \boldsymbol{\nabla}\boldsymbol{\omega}, \tag{1.16}$$

so shall be referred to as the Lighthill–Panton flux tensor. $\boldsymbol{J}'$ is not antisymmetric, so does not have an axial vector representation.
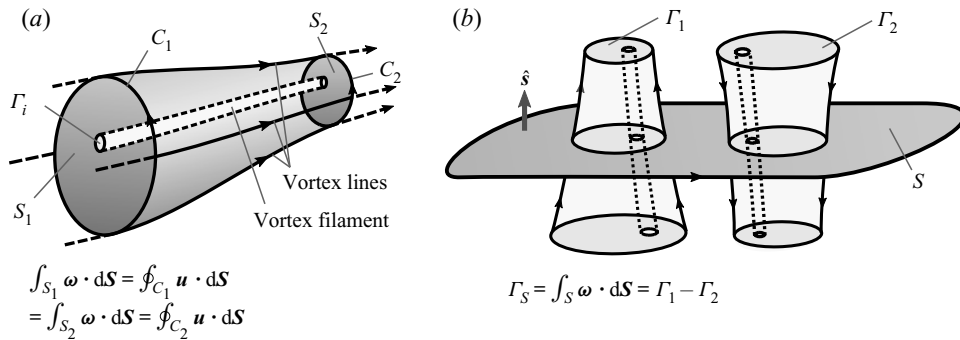
Figure 2. (*a*) The circulation, and flux of vortex lines, is constant along the length of a vortex tube. We consider this tube to comprise a bundle of 'vortex filaments' – thin vortex tubes of infinitesimal circulation, with Γ_i representing the circulation contained in the '*i*'-th filament. (*b*) The total circulation in S is equal to the sum of circulations of all vortex tubes passing through S. If each vortex tube is interpreted as a bundle of vortex filaments, then Γ_S is a measure of the net strength of all filaments passing through S.

In this section, we have shown that Lyman's definition describes the transfer of circulation due to the tangential viscous acceleration of the fluid, while Lighthill's definition considers only the terms that can lead to a local change in vorticity. While both definitions provide the correct kinematic evolution of the vorticity field, Lyman's definition directly relates the diffusion of vorticity to changes in the velocity field, and therefore directly captures the kinematic relationship between velocity and vorticity.

2. Diffusion of vorticity

An interpretation of the diffusion of vorticity, under Lyman's definition of the vorticity flux, is outlined in this section. This description is motivated by (1.11), where Lyman's flux represents the transfer of normal vorticity across the boundary of a reference surface. This describes how the vortex lines and tubes intersecting the reference surface evolve in time, and can be related to the kinematic condition that vortex lines do not end in the fluid.

The quantity $\int_S \boldsymbol{\omega} \cdot \mathrm{d}\boldsymbol{S}$ in (1.11) is commonly referred to as the 'flux' of vorticity through S, and, by Stokes' theorem, is a measure of the circulation in C,

$$\Gamma_S = \int_S \boldsymbol{\omega} \cdot \mathrm{d}\boldsymbol{S} = \oint_C \boldsymbol{u} \cdot \mathrm{d}\boldsymbol{s}. \tag{2.1}$$

In order to distinguish this quantity from the boundary vorticity flux, it shall be referred to as the 'flux of vortex lines' through S. Γ_S is a measure of the amount of vorticity passing through S, and is equal to the net circulation of all vortex tubes passing through S. It is well known that vortex lines do not end within the fluid, except at null points where the vorticity is zero (Fuentes 2007). Furthermore, the strength (circulation) of a vortex tube is constant along its length, and Γ_S is the same for any cross-section or boundary contour of the tube. Now, we might imagine each vortex tube to be divided into infinitesimal vortex filaments, each being a thin vortex tube of infinitesimal circulation, as illustrated in figure 2(*a*). Γ_S then provides the total strength of all vortex filaments passing through S (figure 2*b*), and Lyman's flux in (1.11) provides the rate of transport of vortex filaments across ∂S by viscous diffusion.

The structure of this section is as follows: in § 2.1, a general form of (1.11) is presented and discussed. The role of Lyman's flux in this equation, describing the transfer of vortex filaments along a reference surface, is discussed in § 2.2. This interpretation of

Lyman's flux is applied to viscous vortex connection in § 2.3, where it is demonstrated that Lyman's flux provides a clear mechanism for enforcing the kinematic condition that vortex lines do not end in a fluid. Finally, in § 2.4, the axial flux vector is expressed in 'vortex-line coordinates', illustrating various aspects of vortex line geometry that influence the diffusion of vorticity.

2.1. *An evolution equation for the flux of vortex lines through S*

An expression for the balance of circulation in a two-dimensional control surface is outlined in this section. This control surface formulation is a powerful tool for analysing fully three-dimensional vorticity fields, as demonstrated in § 4.2. The following generalisation of (1.11) is derived in Appendix A:

$$\frac{\mathrm{d}\Gamma_s}{\mathrm{d}t} = \frac{\mathrm{d}}{\mathrm{d}t} \int_S \boldsymbol{\omega} \cdot \mathrm{d}\boldsymbol{S} = \oint_C \left[\hat{\boldsymbol{n}} \times \left[(\boldsymbol{u} - \boldsymbol{v}^b) \times \boldsymbol{\omega} - \nu(\nabla \times \boldsymbol{\omega}) \right] \right] \cdot \hat{\boldsymbol{s}} \, \mathrm{d}s, \qquad (2.2)$$

where $\boldsymbol{v}^b$ is the boundary velocity. The integrand is similar to the vorticity flux in (1.14), and we introduce the modified axial flux vector,

$$\boldsymbol{j}^* = -(\boldsymbol{u} - \boldsymbol{v}^b) \times \boldsymbol{\omega} + \nu\nabla \times \boldsymbol{\omega}, \qquad (2.3)$$

which includes motion of the control surface. As in (1.14), the viscous part of $\hat{\boldsymbol{n}} \times \boldsymbol{j}^*$ is Lyman's flux, $\nu\hat{\boldsymbol{n}} \times (\nabla \times \boldsymbol{\omega})$. Also, $\hat{\boldsymbol{n}} \times \boldsymbol{j}^*$ indicates the transfer of vorticity in the $\hat{\boldsymbol{n}}$-direction, by both viscous forces, and advection relative to the moving surface.

Equation (2.2) can also be expressed in terms of the surface divergence of the 'surface flux vector', $\hat{\boldsymbol{s}} \times \boldsymbol{j}^*$. First, since $(\hat{\boldsymbol{n}} \times \boldsymbol{j}^*) \cdot \hat{\boldsymbol{s}} = -(\hat{\boldsymbol{s}} \times \boldsymbol{j}^*) \cdot \hat{\boldsymbol{n}}$, the following expressions are obtained:

$$\frac{\mathrm{d}\Gamma_s}{\mathrm{d}t} = -\oint_C (\hat{\boldsymbol{n}} \times \boldsymbol{j}^*) \cdot \hat{\boldsymbol{s}} \, \mathrm{d}s = \oint_C (\hat{\boldsymbol{s}} \times \boldsymbol{j}^*) \cdot \hat{\boldsymbol{n}} \, \mathrm{d}s = -\oint_C \boldsymbol{j}^* \cdot \mathrm{d}\boldsymbol{s} = -\int_S (\nabla \times \boldsymbol{j}^*) \cdot \mathrm{d}\boldsymbol{S}. \tag{2.4}$$

Using a surface-moving frame (Wu 1995), the final term is cast into surface divergence form,

$$\hat{\boldsymbol{s}} \cdot (\nabla \times \boldsymbol{j}^*) = \hat{\boldsymbol{s}} \cdot (\boldsymbol{r}^\alpha \times \boldsymbol{j}_{,\alpha}^*) = \boldsymbol{r}^\alpha \cdot (\boldsymbol{j}_{,\alpha}^* \times \hat{\boldsymbol{s}}) = \boldsymbol{r}^\alpha \cdot (\boldsymbol{j} \times \hat{\boldsymbol{s}})_{,\alpha} = -\nabla_S \cdot (\hat{\boldsymbol{s}} \times \boldsymbol{j}^*), \quad (2.5)$$

where ∇_S is the surface-tangent component of the gradient operator (Wu 1995), and the following surface-divergence conservation law is obtained:

$$\frac{\mathrm{d}\Gamma_s}{\mathrm{d}t} = \int_S \nabla_S \cdot (\hat{\boldsymbol{s}} \times \boldsymbol{j}^*) \, \mathrm{d}S = \oint_C \hat{\boldsymbol{n}} \cdot (\hat{\boldsymbol{s}} \times \boldsymbol{j}^*) \, \mathrm{d}s. \tag{2.6}$$

According to (2.6), the surface flux vector, $\hat{\boldsymbol{s}} \times \boldsymbol{j}^*$, describes the local flux of $\hat{\boldsymbol{\omega}} \cdot \hat{\boldsymbol{s}}$ along S, and $\hat{\boldsymbol{n}} \cdot (\hat{\boldsymbol{s}} \times \boldsymbol{j}^*)$ provides the rate of transport across the boundary curve, C. Given the interpretation of Γ_S as the flux of vortex filaments through S, (2.2), (2.4) and (2.6) are equivalent forms of a transport equation for the flux of vortex filaments through any arbitrary reference surface S – they describe how the distribution of vortex filaments passing through S evolves in time. Huggins & Bacon (1980) and Huggins (1994) provide a similar interpretation of the Lyman–Huggins tensor ($\boldsymbol{J}$). They express the vorticity flux as a conservation law for the vorticity intersecting a two-dimensional plane, and relate this conservation law to the intersection of vortex cores with the plane. Our interpretation of (2.4) extends this result to curved and deforming reference surfaces.
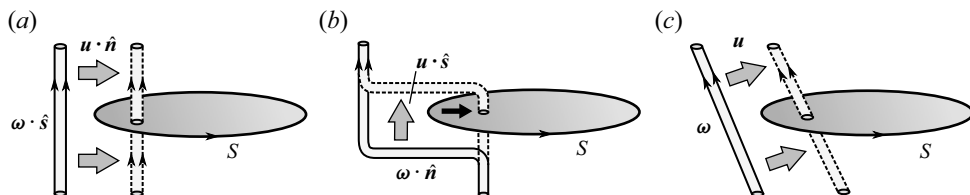
Figure 3. Advection of vortex filaments across the boundary of a stationary reference surface. (*a*) Advection of normal vorticity in the tangential direction, $(\boldsymbol{\omega} \cdot \hat{\boldsymbol{s}})(\boldsymbol{u} \cdot \hat{\boldsymbol{n}})$. (*b*) Advection of tangential vorticity in the normal direction, $(\boldsymbol{\omega} \cdot \hat{\boldsymbol{n}})(\boldsymbol{u} \cdot \hat{\boldsymbol{s}})$. (*c*) Advection of an oblique vortex filament across the boundary.

Some care must be taken with this interpretation. Vortex filaments do not generally evolve in a topologically well-defined manner, and Γ_S describes only the local intersection of vortex filaments with S. Furthermore, Fuentes (2007) has pointed out that vortex tubes (and hence, filaments) may be self-intersecting, and may split apart at null points in the vorticity field. It must be stressed that vortex filaments are invoked only to aid interpretation. Lyman's flux describes the diffusion of vorticity, and not of vortex filaments, and is not affected by these concerns.

2.2. *Advection and diffusion of vortex lines*

We now proceed to provide a physical interpretation of the vorticity flux in (2.4). Introducing the relative velocity, $\boldsymbol{u}^* = (\boldsymbol{u} - \boldsymbol{v}^{\mathbf{b}})$, the axial flux vector ((2.3)) includes the following terms:

$$\hat{\boldsymbol{s}} \cdot (\hat{\boldsymbol{n}} \times \boldsymbol{j}^*) = -\hat{\boldsymbol{n}} \cdot (\hat{\boldsymbol{s}} \times \boldsymbol{j}^*)$$
$$= (\boldsymbol{\omega} \cdot \hat{\boldsymbol{s}})(\boldsymbol{u}^* \cdot \hat{\boldsymbol{n}}) - (\boldsymbol{\omega} \cdot \hat{\boldsymbol{n}})(\boldsymbol{u}^* \cdot \hat{\boldsymbol{s}}) - \nu \left[\hat{\boldsymbol{n}} \cdot \nabla \boldsymbol{\omega} \cdot \hat{\boldsymbol{s}} - \hat{\boldsymbol{s}} \cdot \nabla \boldsymbol{\omega} \cdot \hat{\boldsymbol{n}} \right]. \quad (2.7)$$

The advection terms are considered first, as these have a well-accepted interpretation: in inviscid flows, vortex tubes remain material tubes, and are advected with the flow. For inviscid flow ($\nu = 0$) and a stationary surface ($\boldsymbol{u}^* = \boldsymbol{u}$), (2.2) reduces to

$$\frac{\mathrm{d}\Gamma_s}{\mathrm{d}t} = \oint_C \left[(\boldsymbol{\omega} \cdot \hat{\boldsymbol{n}})(\boldsymbol{u} \cdot \hat{\boldsymbol{s}}) - (\boldsymbol{\omega} \cdot \hat{\boldsymbol{s}})(\boldsymbol{u} \cdot \hat{\boldsymbol{n}}) \right] \mathrm{d}s. \quad (2.8)$$

The second term in the integral, $(\boldsymbol{\omega} \cdot \hat{\boldsymbol{s}})(\boldsymbol{u} \cdot \hat{\boldsymbol{n}})$, represents the advection of vortex lines normal to S in a direction tangent to S, as illustrated in figure 3(*a*). The first term in the integral, $(\boldsymbol{\omega} \cdot \hat{\boldsymbol{n}})(\boldsymbol{u} \cdot \hat{\boldsymbol{s}})$, represents the advection of tangent vorticity across S in the normal direction. As demonstrated in figure 3(*b*), this process also results in a change in the density of vortex filaments passing through S, unless the entire vortex filament is advected across the surface. A similar observation on this longitudinal advection term was made by Huggins & Bacon (1980). In general, of course, vortex lines intersect S at an oblique angle, and both terms occur simultaneously (figure 3*c*).

The Lyman–Huggins tensor, $\boldsymbol{J}$, is antisymmetric, and each term in the axial vector, $\boldsymbol{j}$, occurs twice in the full tensor – once representing the transfer of normal vorticity in a direction tangent to S, and second as the transfer of tangential vorticity in a direction normal to S. If we consider a second surface, N, which intersects S orthogonally, as illustrated in figure 4, each term in (2.7) describes vorticity transport in both surfaces. The term $(\boldsymbol{\omega} \cdot \hat{\boldsymbol{s}})(\boldsymbol{u} \cdot \hat{\boldsymbol{n}})$ appears in the transport equation for $\boldsymbol{\omega} \cdot \hat{\boldsymbol{s}}$ in S, where it represents the advection of vorticity along S (the primary effect). The same term also appears in the transport equation for $\boldsymbol{\omega} \cdot \hat{\boldsymbol{n}}$ in N, where it describes the advection of tangential
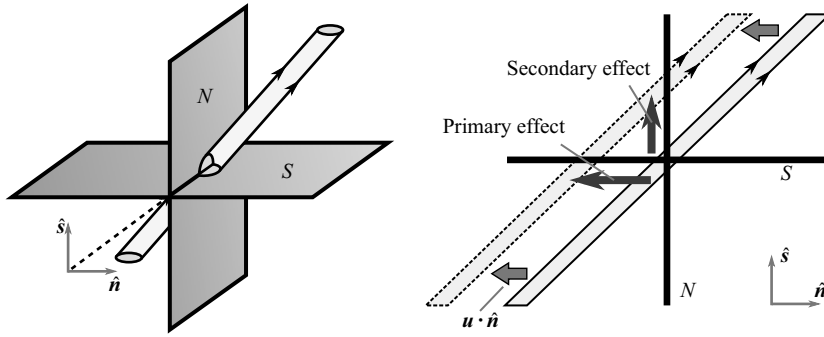
Figure 4. Transport of a vortex filament through two orthogonally intersecting surfaces. The term $(\boldsymbol{\omega} \cdot \hat{\boldsymbol{s}})(\boldsymbol{u} \cdot \hat{\boldsymbol{n}})$ occurs twice in the flux tensor, once representing the transport of $(\boldsymbol{\omega} \cdot \hat{\boldsymbol{s}})$ in the $\hat{\boldsymbol{n}}$-direction (the primary effect), and a second time as the transport of $(\boldsymbol{\omega} \cdot \hat{\boldsymbol{n}})$ in the $\hat{\boldsymbol{s}}$-direction (the secondary effect). Viscous terms in the Lyman–Huggins tensor are interpreted in an analogous manner.

vorticity across N (the secondary effect). The primary effect corresponds to the standard interpretation of $(\boldsymbol{\omega} \cdot \hat{\boldsymbol{s}})(\boldsymbol{u} \cdot \hat{\boldsymbol{n}})$ as an advective flux, while the secondary effect represents the consequences of this advection on the $\boldsymbol{\omega} \cdot \hat{\boldsymbol{n}}$ field.

The primary and secondary effects of the viscous fluxes in (2.7) are defined in an analogous manner. The primary effect of the term $-\nu \hat{\boldsymbol{n}} \cdot \nabla \boldsymbol{\omega} \cdot \hat{\boldsymbol{s}}$ is the diffusion of $\boldsymbol{\omega} \cdot \hat{\boldsymbol{s}}$ in the $\hat{\boldsymbol{n}}$-direction, and is equivalent to the diffusion of vorticity under Lighthill's definition. However, this term also produces a secondary diffusion of $\boldsymbol{\omega} \cdot \hat{\boldsymbol{n}}$ in the $\hat{\boldsymbol{s}}$-direction, which does not appear in Lighthill's definition. In the next section, we illustrate that the secondary viscous effect can be interpreted as due to the kinematic condition that vortex filaments do not end inside the fluid.

2.3. *Vortex reconnection*

Vortex reconnection across an 'X'-point/line is examined in this section, where we demonstrate that Lyman's flux provides a measure of the rate at which vorticity is reconnected across the 'X'-line. Moreover, Lyman's definition clearly illustrates how the kinematic condition that vortex lines and filaments do not end inside the fluid (except at null points) is maintained during the reconnection process. Nether of these benefits is afforded by Lighthill's definition. A two-dimensional model problem, Kida & Takaoka's (1991) straight jet flow (their example (*d*)), is considered first. Then, the three-dimensional interaction of antiparallel vortex pairs is briefly discussed.

The straight jet flow is an analytic solution to the Navier–Stokes equations, featuring vortex reconnection in two-dimensions. Expressions for the velocity and vorticity fields are provided by Kida & Takaoka (1991), and are of the following form,

$$\boldsymbol{u}(x, y, t) = (-Ax, 0, Az + \bar{u}_z(x, y, t)), \tag{2.9a}$$

$$\boldsymbol{\omega}(x, y, t) = \left(\frac{\partial \bar{u}_z}{\partial y}, -\frac{\partial \bar{u}_z}{\partial x}, 0 \right). \tag{2.9b}$$

Vorticity vectors, as well as closed vortex lines (contours of $\bar{u}_z$), are provided in figure 5, for a selection of time instants, and a transient animation is also provided in supplementary movie 1 available at https://doi.org/10.1017/jfm.2021.179. The initial vorticity field features two nodes ('O'-points), labelled C and C', and a saddle ('X'-point) at A. Closed vortex lines either orbit a single node (island) or the entire set of both nodes and the saddle point.
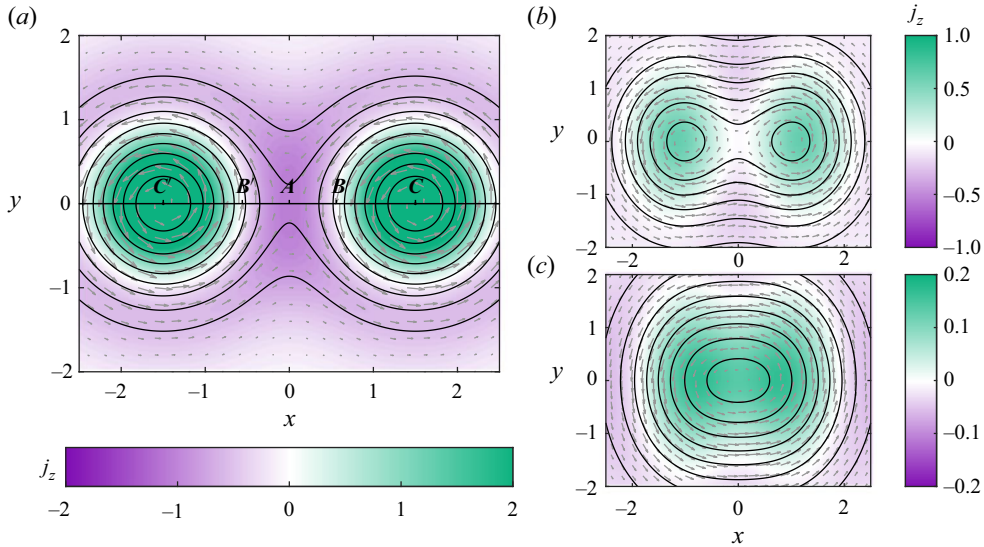
Figure 5. The two-dimensional vorticity field of Takaoka's straight jet flow, at (*a*) $t = 0$, (*b*) $t = 0.3$ and (*c*) $t = 0.6$. Light-grey vectors represent the vorticity field, while solid lines are closed vortex lines. Colour shading indicates the viscous part of the axial flux vector, j_z.

During transient evolution, vorticity flux (meaning the flux of vortex lines) is annihilated at the centre of each island, while vortex reconnection occurs at the saddle point, transferring vorticity flux from each island (C and C') to the outer orbit ($C'AC$). At the critical time, $t \approx 0.506$, the two nodes and the saddle point merge into a single node.

Topological changes to the vorticity field, including vortex reconnection and the annihilation of flux, are driven by viscous diffusion. These particular topological processes have previously been described by Melander & Hussain (1990) and Greene (1993). Here, the role of Lyman's flux in interpreting these processes is clarified.

Since the vorticity field is two-dimensional, the axial flux vector, $\boldsymbol{j}$, has only a single non-zero component. As advection is not responsible for topological changes to the vorticity field, the following discussion is largely concerned with the viscous part of the flux vector,

$$j_z = \nu \left[\frac{\partial \omega_y}{\partial x} - \frac{\partial \omega_x}{\partial y} \right], \tag{2.10}$$

which is indicated by colour shading in figure 5. Note that j_z simultaneously describes the rate of transport of ω_x in the y-direction and of ω_y in the x-direction. Specifically, $j_z > 0$ indicates the transport of positive ω_x in the positive y-direction (or negative ω_x in the negative y-direction) and the transfer of positive ω_y in the negative x-direction (or negative ω_y in the positive x-direction). For $j_z < 0$, vorticity transport occurs in the opposite direction.

Consider the section of the x-axis between A and C, as illustrated in figure 6(*a*). The arrows on this figure indicate the direction of vorticity transport, determined by the sign of j_z. Between A and B, $j_z < 0$, and negative ω_y is diffused in the negative x-direction, towards A. Simultaneously, opposite-signed ω_x is diffused away from the x-axis in the vertical direction, with negative ω_x above the x-axis and positive ω_x below the x-axis. Between B and C, $j_z > 0$, and negative ω_y is diffused in the positive x-direction, towards C. Simultaneously, opposite-signed ω_x is diffused towards the x-axis from above and below.
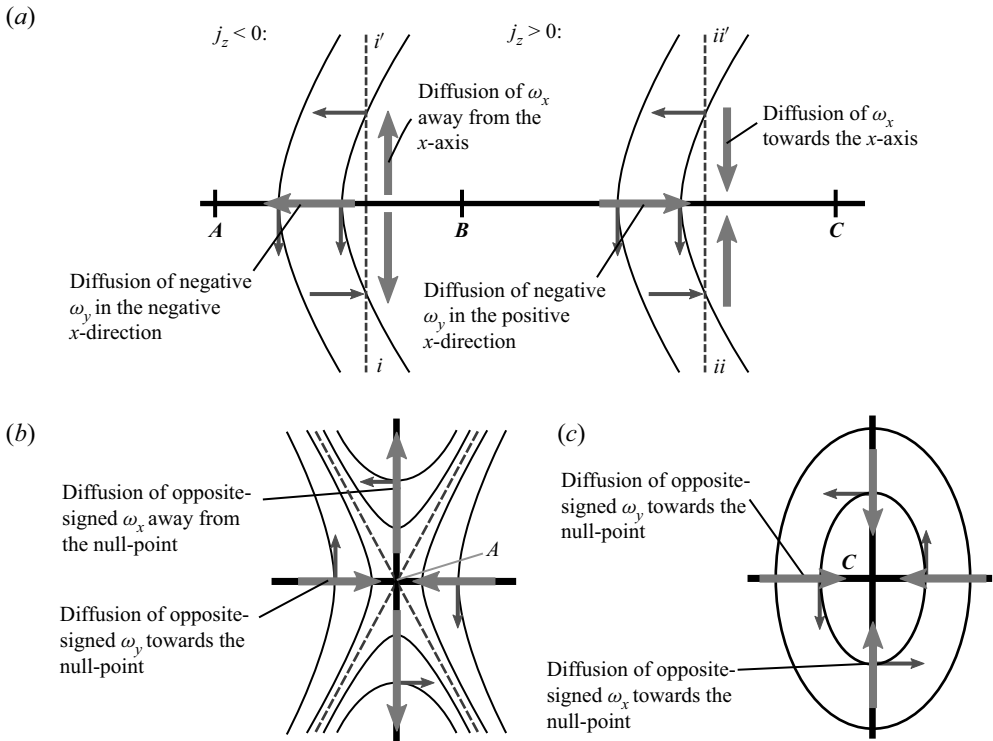
915 A106-11

Figure 6. Schematic illustration of the diffusion of vorticity in the straight jet flow: (*a*) Along the section of the *x*-axis between *A* and *C*, $j_z < 0$ results in the diffusion of negative ω_y to the left, accompanied by the diffusion of opposite-signed ω_x away from the *x*-axis. When $j_z > 0$, negative ω_y is diffused to the right, with corresponding diffusion of opposite-signed ω_x towards the *x*-axis. (*b*) Opposite-signed ω_y is diffused towards the 'X'-point (*A*), where cross-diffusive annihilation occurs. Vortex lines are reconnected across the *y*-axis, as opposite-signed ω_x diffuses away from the null-point. (*c*) Annihilation of flux loops about an 'O'-point (*C*), as opposite-signed ω_y cross-annihilates along the *x*-axis, and opposite-signed ω_x cross-annihilates on the *y*-axis.

The coupling between the fluxes of ω_x and ω_y can be understood as due to the kinematic condition that vortex filaments do not end inside the fluid, except at vorticity nulls. The diffusion of negative ω_y across the line $i - i'$ in figure 6(*a*) effectively results in the transport of a vortex filament across this line. In order for this filament to remain connected to itself, new ω_x must appear in $i - i'$, both above and below the *x*-axis, and this is guaranteed by Lyman's flux. Under Lighthill's flux, however, the transport equations for ω_x and ω_y are effectively independent, and the appearance of new ω_x in $i - i'$ is unrelated to the diffusion of ω_y.

The annihilation of vorticity at the node, *C*, is illustrated in figure 6(*c*). Here $j_z > 0$, driving the diffusion of negative ω_y towards *C* from the left and positive ω_y towards *C* from the right. Cross-annihilation of opposite-signed ω_y is therefore occurring at *C*. Similarly, opposite-signed ω_x is cross-annihilated on *C*, with negative ω_x diffused towards *C* from above and positive ω_x diffused towards *C* from below. The total flux of vortex lines orbiting *C* therefore decreases, owing to the annihilation of closed flux loops as they diffuse into the centre of the node. Lyman's flux not only describes the qualitative physical features of this process but also provides a direct measure of the rate of annihilation.

Finally, the reconnection of vortex lines at the saddle point, *A*, is illustrated in figure 6(*b*). Here, $j_z < 0$, driving the diffusion of opposite-signed ω_y towards *A*, where viscous

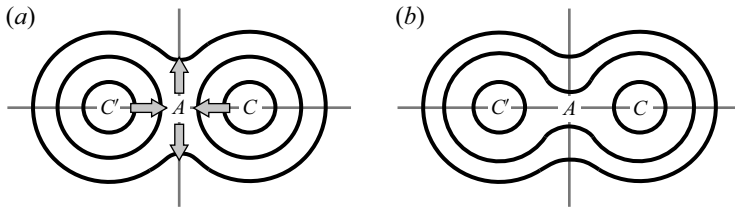(*a*)   (*b*)

Figure 7. The reconnection of vortex lines across the 'X'-point. The cross-diffusive annihilation of opposite-sign ω_y on the *x*-axis reduces the 'flux of vortex lines' passing through the *x*-axis, and this is balanced by the cross-diffusion of opposite-signed ω_x away from *A*, along the *y*-axis. Antiparallel vortex lines passing through the *x*-axis are 'cut' by the cross-annihilation of ω_y, and reconnected across the *y*-axis by the cross-diffusion of opposite-signed ω_x away from *A*.

cross-annihilation occurs. However, because ω_x is positive below the *x*-axis and negative above it, $j_z < 0$ indicates the diffusion of opposite-signed ω_x away from *A* along the *y*-axis, effectively creating new vorticity in the *y*-axis. As illustrated in figure 7, the flux of vortex lines passing through the *x*-axis is reduced by the cross-diffusive annihilation of ω_y, and this is balanced by an increase in the flux of vortex lines passing through the *y*-axis. Vortex lines passing through the *x*-axis are 'cut' by the cross-annihilation of ω_y, and reconnected across the *y*-axis by the cross-diffusion of ω_x away from *A*. Saffman (1990) has stressed that the cutting and reconnection of vortex lines should not be seen as separate processes; instead, reconnection must occur as a 'consequence of the kinematic theorem that vortex lines cannot end inside a fluid'. Lyman's flux allows the cross-annihilation and reconnection of vortex lines to be described by the same component of the axial flux vector, and it therefore directly captures this important property of the vorticity field.

The interaction of antiparallel vortex pairs, illustrated in figure 8, features a three-dimensional 'X'-line reconnection. Detailed analysis and numerical simulation of this flow is provided by, for example, Melander & Hussain (1989, 1990) and McGavin & Pontin (2018), and only a brief description is presented here. The main feature of the connection process is the transfer of circulation from the symmetry plane (C_s) to the dividing plane (C_d). At the contact zone, vortex filaments are cut by viscous cross-annihilation and are reconnected across the dividing plane, forming the bridge structures in figure 8(*c*). While most of the circulation is transferred by this 'cut-and-connect' process, a small amount of circulation remains in the threads (figure 8*d*), which persist long after the main reconnection process has ended.

The reconnection process is governed by the value of Lyman's flux along the connection line (the intersection between the symmetry and dividing planes, $C_s \cap C_d$),

$$\hat{d} \cdot \boldsymbol{J} \cdot \hat{s} = -\hat{s} \cdot \boldsymbol{J} \cdot \hat{d} = -\nu \left[\hat{d} \cdot \nabla \boldsymbol{\omega} \cdot \hat{s} - \hat{s} \cdot \nabla \boldsymbol{\omega} \cdot \hat{d} \right]. \tag{2.11}$$

This term simultaneously describes the rate at which $\boldsymbol{\omega} \cdot \hat{s}$ is cross-annihilated on the symmetry plane (the cutting of vortex filaments), and at which opposite-signed $\boldsymbol{\omega} \cdot \hat{d}$ is diffused away from the connection line (vortex reconnection). The loss of circulation from C_s is directly balanced by the appearance of new circulation in C_d, and Lyman's flux provides a direct measure of this process. In fact, expressions equivalent to Lyman's flux have previously been used to measure the rate of circulation, in both vortex ring (Stanaway, Shariff & Hussain 1988), and vortex pair (McGavin & Pontin 2018) interactions.

It should be stressed that for vortex reconnections without symmetry, such as high-Reynolds number and off-axis reconnections (Beardsell, Dufresne & Dumas 2016), the extent of reconnection is not accurately represented by the circulation transfer.
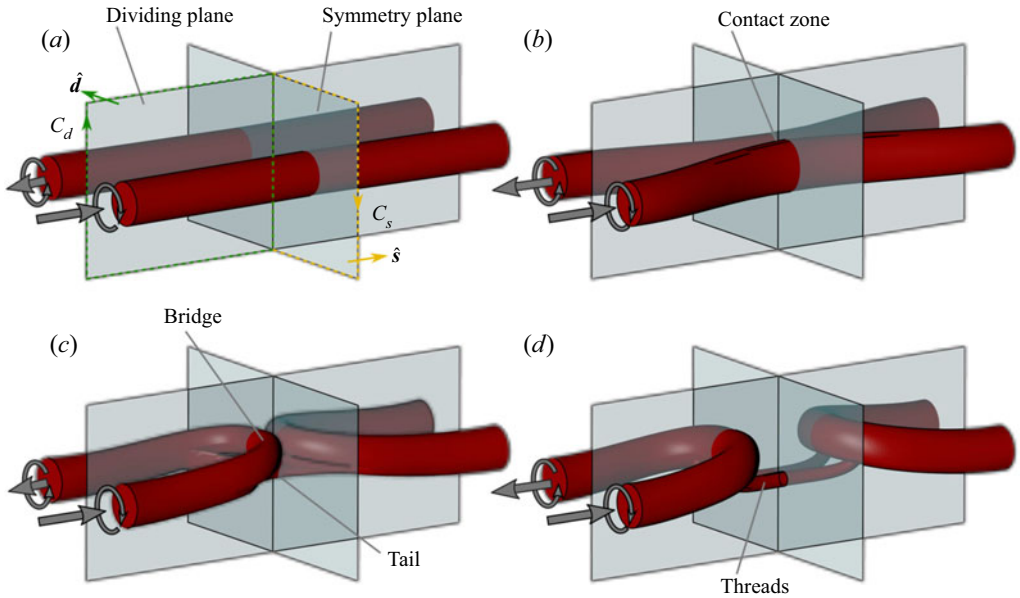
Figure 8. Illustration of the 'bridging' mechanism for the reconnection of an antiparallel vortex pair, based on the description provided by Melander & Hussain (1989, 1990). (*a*–*d*) Three-dimensional isometric view showing the main features of vortex tubes at several instances during the connection process. These images are merely representative of flow behaviour; for accurate numerical data, see Melander & Hussain (1989, 1990) or McGavin & Pontin (2018).

Lyman's flux still governs the transfer of circulation between the symmetry and dividing planes; however, this does not necessarily correspond to the rate of reconnection in asymetric cases.

In this section, we have illustrated that Lyman's flux can provide a measure of the rate of reconnection at 'X'-points, and of the annihilation of vortex loops at 'O' points. Moreover, the coupling between the fluxes of each component of vorticity, which occurs under Lyman's definition, can be interpreted as a consequence of the solenoidal property of the vorticity field, which requires that vortex lines and filaments do not end in the fluid, apart form at null points. The solenoidal property is a consequence of the definition of vorticity as the curl of velocity, and Lyman's flux clearly illustrates how this condition is enforced – a benefit which is not afforded by Lighthill's definition.

2.4. *Vortex line coordinates*

In this section, the viscous part of the axial flux vector is decomposed into components normal and tangent to vortex lines, to provide some insight into how the geometry of vortex lines impacts the diffusion of vorticity. In a fluid region where $\boldsymbol{\omega} \neq 0$, let ω be the vorticity magnitude, and $\hat{\boldsymbol{b}}$ be a unit vector tangent to the vorticity field ($\boldsymbol{\omega} = \omega\hat{\boldsymbol{b}}$). Then, the components of the axial flux vector either tangent or normal to $\hat{\boldsymbol{b}}$ are

$$-\nu\hat{\boldsymbol{b}} \times (\boldsymbol{\nabla} \times \boldsymbol{\omega}) = -\nu\left[\boldsymbol{\nabla}_{\perp}\omega - \omega\frac{\partial\hat{\boldsymbol{b}}}{\partial b}\right], \qquad (2.12a)$$

$$-\nu\hat{\boldsymbol{b}} \cdot (\boldsymbol{\nabla} \times \boldsymbol{\omega}) = -\nu\omega\hat{\boldsymbol{b}} \cdot (\boldsymbol{\nabla} \times \hat{\boldsymbol{b}}), \qquad (2.12b)$$
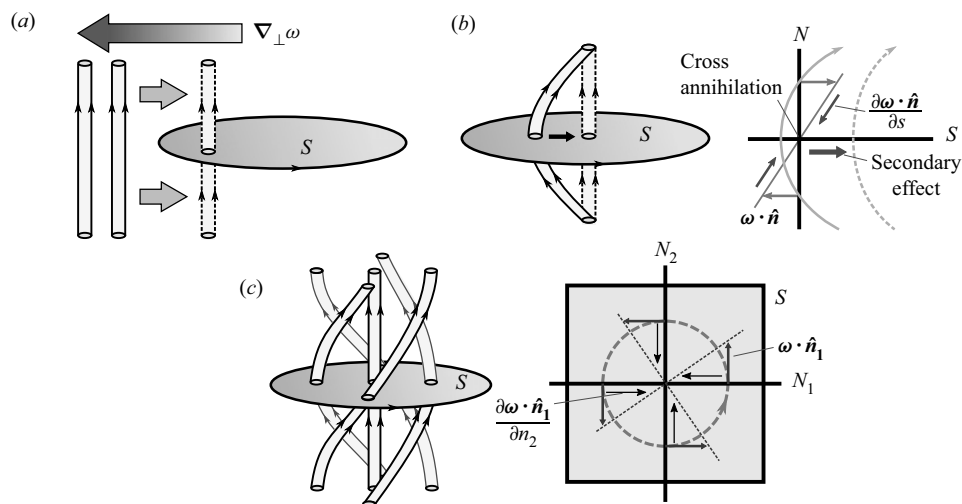
Figure 9. The three terms in the axial flux vector when expressed in local vorticity coordinates: (*a*) Diffusion of vortex-tangential vorticity in the vortex-normal direction due to gradients in vorticity magnitude. (*b*) Diffusion of vortex-tangential vorticity due to vortex line curvature. This can be interpreted as a consequence of the cross-diffusion of vortex normal vorticity in the vortex-tangent direction. (*c*) Cross-diffusion of vortex-normal vorticity, due to the torsion of vortex lines. This term is also related to the generation or dissipation of helicity.

where $\nabla_\perp$ is the projection of the gradient operator on the plane with unit normal $\hat{\boldsymbol{b}}$, $\nabla_\perp \omega = \nabla \omega - \hat{\boldsymbol{b}}(\cdot \nabla \omega)\hat{\boldsymbol{b}}$. Equation (2.12*a*) gives the components of the axial flux vector which are orthogonal to the vorticity vector, and therefore simultaneously describes the diffusion of vortex-tangent vorticity (the component of vorticity parallel to the local vorticity vector) in directions orthogonal to the local vorticity, as well as the diffusion of vortex-normal vorticity (the components of vorticity orthogonal to the local vorticity vector) in the direction parallel to the vorticity vector. Equation (2.12*b*) provides the component of the axial flux vector tangent to the local vorticity vector, which describes the diffusion of vortex-normal vorticity in directions orthogonal to the local vorticity vector. Obviously, the vortex-normal vorticity is zero at any given point. However, as neighbouring vortex lines are not necessarily parallel, spatial gradients in the component of vorticity orthogonal to the local vorticity vector may occur, producing a diffusive flux of vortex-normal vorticity.

This decomposition reveals three aspects of vortex line geometry which contribute to the diffusion of vorticity. The first is the diffusion of vortex-tangential vorticity, in directions orthogonal to the vorticity vector, due to gradients in the vorticity magnitude. This effect is illustrated in figure 9(*a*), and is the only mechanism which operates in two-dimensional flows.

The second effect is due to the curvature of vortex lines ($\partial \hat{\boldsymbol{b}}/\partial b$), which also drives the diffusion of vortex-tangent vorticity in directions orthogonal to the vortex line, as illustrated in figure 9(*b*). This can be interpreted as a secondary effect, driven by the cross-diffusion of opposite-signed vortex-normal vorticity. In figure 9(*b*), positive $\boldsymbol{\omega} \cdot \hat{\boldsymbol{n}}$ diffuses along N, towards S from above, while negative $\boldsymbol{\omega} \cdot \hat{\boldsymbol{n}}$ diffuses from below. The cancellation of opposite-signed vorticity in N is also associated with the secondary diffusion of vortex-line tangent vorticity along S.

The final effect is related to the torsion of vortex lines, where $\hat{\boldsymbol{b}} \cdot (\nabla \times \hat{\boldsymbol{b}})$ is non-zero, as illustrated in figure 9(*c*). This term acts to diffuse vortex-normal vorticity in directions orthogonal to the local vorticity vector, as illustrated in figure 9(*c*). Here, S is the plane formed with a normal vector, $\hat{\boldsymbol{b}}_0$, at a particular reference point. At this reference point, $\nu\omega\hat{\boldsymbol{b}}_0 \cdot (\nabla \times \hat{\boldsymbol{b}})$ describes the diffusion of vorticity in the planes N_1 and N_2, which are orthogonal to S. Analogous to the annihilation of flux at a two-dimensional 'O'-point, opposite-signed $\boldsymbol{\omega} \cdot \hat{\boldsymbol{n}}_1$ in the N_1 plane is cross-annihilated at the origin, and $\boldsymbol{\omega} \cdot \hat{\boldsymbol{n}}_2$ in the N_2 plane is also cross-annihilated. Of course, the tangential vorticity field may resemble a two-dimensional 'X'-point, rather than the 'O'-point shown in figure 9(*c*). Furthermore, $\hat{\boldsymbol{b}}_0$ was arbitrarily selected, and similar cross-diffusion of normal vorticity occurs about all vortex lines where $\hat{\boldsymbol{b}} \cdot (\nabla \times \hat{\boldsymbol{b}}) \neq 0$.

This term is also related to the viscous generation and dissipation of helicity. The helicity source term, $\nu\boldsymbol{\omega} \cdot (\nabla \times \boldsymbol{\omega})$ (Kida & Takaoka 1994; Takaoka 1996), is proportional to the component of the axial flux vector aligned with the local vorticity vector. Clearly, the cross-diffusion of vortex-line normal vorticity, driven by the vortex-line tangent component of the axial flux vector, plays an important role in the generation or dissipation of helicity.

3. Generation of vorticity

In this section, we present a three-dimensional extension of Morton's (1984) inviscid theory of vorticity creation. Under this formulation, circulation is generated on an interface by the inviscid relative acceleration between fluid elements and the solid boundary, due to either tangential acceleration of the solid boundary or tangential pressure gradients and body forces in the fluid. Viscosity is responsible for the diffusion of vorticity into the fluid after it has been generated, but is not involved in the vorticity creation process.

The inviscid description of vorticity generation has been controversial. In particular, Wu & Wu (1993, 1996) and Wu (1995) have argued that viscosity is essential to the vorticity creation process. Inviscid formulations, such as those of Morton (1984), Morino (1986), Brøns *et al.* (2014) and Terrington *et al.* (2020), interpret the velocity discontinuity across a free-slip boundary as an 'interface vortex sheet', and treat it as part of the vorticity field. However, Wu & Wu (1993) argue that the interface vortex sheet does not correspond to the rotation of fluid elements, and therefore does not represent a layer of vorticity on the boundary. More precisely, vorticity corresponds to rotation of the principal rate-of-strain axes, and the principal axes do not necessarily rotate on a free-slip boundary.

These observations necessitate a distinction between boundary vorticity and the interface vortex sheet. Boundary vorticity represents the rotation of fluid elements on the boundary, and is computed from gradients in the fluid velocity. The interface vortex sheet corresponds to circulation contained in the velocity discontinuity at the boundary, as fluid elements slide along the boundary, and is not related to fluid rotation. By maintaining this distinction, Wu & Wu's observations do not contradict the inviscid model of vorticity creation.

Including the interface vortex sheet as part of the vorticity field is a conceptually attractive approach, as it allows the generation of vorticity to be decoupled from its subsequent diffusion (Morton 1984), as well as admitting a general description of vorticity creation, applicable to both no-slip and free-slip boundaries (Terrington *et al.* 2020). Moreover, the interface vortex sheet generalises several kinematic properties of the vorticity field across tangential discontinuities (§ 3.2), providing further justification for the inviscid description of vorticity generation.
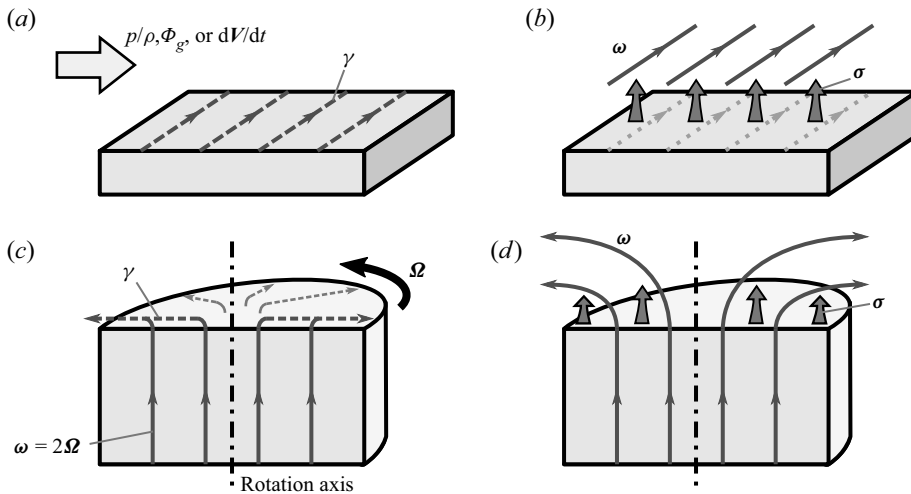
Figure 10. Schematic illustration of the proposed vorticity generation mechanism. Circulation is generated in the interface by the inviscid relative acceleration, and diffused into the fluid by the viscous forces which enforce the no-slip condition. (*a,b*) Pressure gradients, body forces and pure translational acceleration generate solenoidal vortex lines, with no change in the normal vorticity on the boundary. (*c,d*) The circulation generated by rotational motion of the solid body ensures that vortex lines are continuous across the boundary.

The structure of this section is as follows: in § 3.1, a qualitative overview of the inviscid description of vorticity creation is presented. Then, in § 3.2, important kinematic properties of the interface circulation are discussed. Finally, further mathematical details of the generation mechanism are provided in § 3.3.

3.1. *Summary of the generation mechanism*

A schematic illustration of the vorticity generation process on a solid boundary is provided in figure 10. Under Morton's (1984) interpretation, the creation of vorticity is interpreted as an inviscid process, independent of the fluid viscosity. In the absence of viscous forces, a relative acceleration between fluid and solid may occur, due to tangential pressure gradients, body forces or external acceleration of the boundary. This produces a velocity discontinuity across the boundary, which is interpreted as a vortex sheet, $\boldsymbol{\gamma} = \hat{\boldsymbol{n}} \times (\boldsymbol{u} - \boldsymbol{v})$. Here, $\boldsymbol{u}$ and $\boldsymbol{v}$ are the velocities of the fluid and solid, respectively, and $\hat{\boldsymbol{n}}$ is the unit normal vector directed out of the solid boundary. The inviscid creation of interface circulation is illustrated in figure 10(*a,c*).

On a no-slip boundary, all circulation generated by the inviscid mechanism is immediately diffused into the fluid by viscous forces, which enforce the no-slip condition, as illustrated in figure 10(*b,d*). Tangential acceleration of the solid boundary, as well as tangential pressure gradients and body forces, produce solenoidal interface circulation (figure 10*a,c*), and the interface circulation diffuses into the fluid without affecting the normal vorticity on the boundary. Rotational acceleration of the solid body, however, produces a uniform vorticity field within the solid body and a non-solenoidal interface circulation. As the interface vortex sheet is diffused into the fluid, the associated diffusion of normal vorticity along the boundary ensures that vortex lines remain continuous across the boundary, as illustrated in figure 10(*b,d*).

Under Lyman's definition of the boundary vorticity flux, normal vorticity is not created on a boundary. While this result is reasonable on stationary boundaries, where the normal

vorticity is zero, it appears to contradict the Dirichlet condition, $\boldsymbol{\omega} \cdot \hat{\boldsymbol{n}} = 2\hat{\boldsymbol{n}} \cdot \boldsymbol{\Omega}$, on a rotating boundary. Although normal vorticity is not created on a rotating boundary, the Dirichlet condition is maintained by the diffusion of normal vorticity along the boundary, due to the secondary effect of the Lyman–Huggins flux tensor. In addition to enforcing the kinematic condition that vortex lines do not end in the fluid interior, the secondary effect also ensures that vortex lines do not end on a solid boundary, enforcing the Dirichlet condition on normal vorticity.

A closely related interpretation of vorticity creation has been widely used in vorticity-based numerical methods (Payne 1956, 1958; Lighthill 1963; Chorin 1973; Leonard 1980), which predate Morton's (1984) interpretation. Each of these authors recognises that vorticity must be introduced at the boundary, in order to satisfy the no-slip condition. Moreover, the amount of vorticity added in each timestep is deduced from the tangential slip velocity that would occur in the absence of vorticity creation. This corresponds to the creation of circulation (slip velocity) by the inviscid relative acceleration, and subsequent diffusion of circulation into the fluid. The success of these methods in capturing the physical behaviour of various flows provides further support for Morton's interpretation of vorticity creation.

3.2. *Kinematic properties of the interface circulation*

Kinematic properties of the interface vortex sheet are discussed here, including a generalised expression for the vector circulation ((3.3)), divergence-free condition ((3.6)) and Biot–Savart law ((3.7)). The results of this section are purely kinematic, and apply to any interface, including the boundary between a fluid and a solid.

The interface circulation is defined by comparison with the vector circulation for a single fluid domain, introduced in (1.9). A control volume, V, which includes an interface, I, between two fluids may be split into two smaller control volumes, V_1 and V_2, as illustrated in figure 11(*a*). This approach is based on the two-dimensional control area formulation presented by Brøns *et al.* (2014) and Terrington *et al.* (2020). The total vector circulation in V may be expressed as

$$\boldsymbol{\Gamma} = \oint_{\partial V} \hat{\boldsymbol{n}} \times \boldsymbol{u} \, \mathrm{d}S = \int_{V_1} \boldsymbol{\omega} \, \mathrm{d}V + \int_{V_2} \boldsymbol{\omega} \, \mathrm{d}V + \int_I \hat{\boldsymbol{s}} \times (\boldsymbol{u}_2 - \boldsymbol{u}_1) \, \mathrm{d}S, \qquad (3.1)$$

where $\boldsymbol{u}_i$ is the velocity of fluid in V_i. The density of circulation in the interface is

$$\boldsymbol{\gamma} = \hat{\boldsymbol{s}} \times (\boldsymbol{u}_2 - \boldsymbol{u}_1), \qquad (3.2)$$

and the total circulation in V includes contributions from vorticity in the fluid interior, as well as circulation due to the velocity discontinuity on the interface,

$$\boldsymbol{\Gamma} = \int_V \boldsymbol{\omega} \, \mathrm{d}V + \int_I \boldsymbol{\gamma} \, \mathrm{d}S. \qquad (3.3)$$

The interface circulation generalises the divergence-free property of the vorticity field across an interface. This can be demonstrated as follows. First, consider Stokes' theorem on each side of the interface,

$$\int_I \boldsymbol{\omega}_i \cdot \mathrm{d}\boldsymbol{S} = \oint_{\partial I} \boldsymbol{u}_i \cdot \mathrm{d}\boldsymbol{s}, \qquad (3.4)$$

where $\boldsymbol{\omega}_i$ is the vorticity in fluid i. The jump in the 'flux of vortex lines' through each side of the interface is

$$\int_I \hat{\boldsymbol{s}} \cdot (\boldsymbol{\omega}_2 - \boldsymbol{\omega}_1) \, \mathrm{d}S = \oint_{\partial I} (\boldsymbol{u}_2 - \boldsymbol{u}_1) \cdot \mathrm{d}\boldsymbol{s} = \oint_{\partial I} \boldsymbol{\gamma} \cdot \hat{\boldsymbol{b}} \, \mathrm{d}s. \qquad (3.5)$$
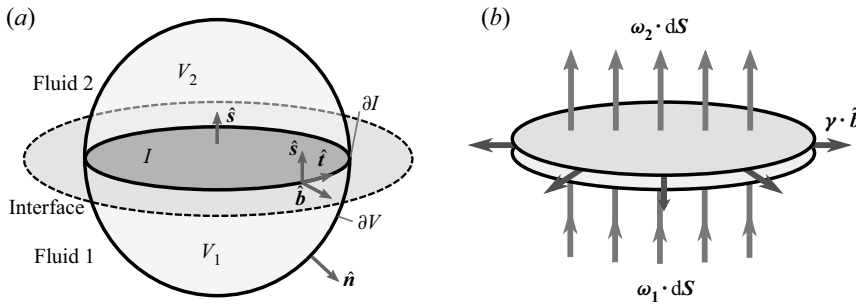
Figure 11. (*a*) Control volume used to analyse the total circulation across an interface, *I*. Here, V_1 and V_2 are the portions of the control volume, *V*, in each fluid; $\hat{\boldsymbol{s}}$ is the unit normal to the interface, and $\hat{\boldsymbol{n}}$ is the unit normal to the control volume boundary, ∂V. $\hat{\boldsymbol{b}}$ is a vector tangent to *I*, but orthogonal to ∂I, and $\hat{\boldsymbol{t}}$ is the tangent to the boundary curve ∂I. (*b*) Illustration of the flux of vortex lines into a section of the interface. The difference in circulation between vortex tubes on each side of the interface is balanced by the flux of circulation along the interface ((3.5)).

Now, $\boldsymbol{\gamma} \cdot \hat{\boldsymbol{b}}$ can be considered the 'flux of interface circulation' through ∂I, and then the generalised divergence theorem for *V* can be expressed as

$$\oint_{\partial V} \boldsymbol{\omega} \cdot \mathrm{d}\boldsymbol{S} + \oint_{\partial I} \boldsymbol{\gamma} \cdot \hat{\boldsymbol{b}} \, \mathrm{d}s = 0, \qquad (3.6)$$

where the sum of the flux of vortex lines, and the flux of interface circulation, across the outer boundary of *V* is equal to zero. This relationship is illustrated in figure 11(*b*). Vortex tubes do not end on a boundary or interface, but either continue across the boundary or as circulation in the interface.

The interface circulation also generalises the Biot–Savart integral to interfaces with slip. The Biot–Savart law is an application of Helmholtz's theorem, which has been extended to general interfaces by Kustepeli (2016). For an incompressible velocity field in an infinite domain, their expression reduces to

$$\boldsymbol{u} = \nabla \times \left[\int_V \frac{\boldsymbol{\omega}}{4\pi R} \, \mathrm{d}V + \int_I \frac{\boldsymbol{\gamma}}{4\pi R} \, \mathrm{d}S \right]. \qquad (3.7)$$

In order to compute the induced velocity field, contributions from the interface vortex sheet must be included, to capture a velocity discontinuity on the interface.

The kinematic properties presented here demonstrate that $\boldsymbol{\gamma}$ generalises the vorticity field across a tangential discontinuity. Using distribution theory, the generalised curl operator is (Kustepeli 2016)

$$\nabla \times \boldsymbol{u} = \{\nabla \times \boldsymbol{u}\} + \boldsymbol{\gamma} \delta(I), \qquad (3.8)$$

where { } denotes the regular value (i.e. the vorticity in each fluid), and $\delta(I)$ is the Dirac delta distribution on *I*. Thus, the interface circulation arises naturally as part of the vorticity field, if distribution theory is used to allow differentiation across the interface. Inviscid formulations of vorticity creation are therefore justified in interpreting the slip velocity as a vortex sheet.

3.3. *The vorticity generation mechanism*

Key mathematical results which support the inviscid interpretation of vorticity creation outlined in § 3.1 are presented here. Let $\boldsymbol{u}$ be the fluid velocity, and $\boldsymbol{v}$ be the velocity of the

solid body, so that the interface circulation is

$$\boldsymbol{\gamma} = \hat{\boldsymbol{n}} \times (\boldsymbol{u} - \boldsymbol{v}), \qquad (3.9)$$

where $\hat{\boldsymbol{n}}$ is the unit normal directed out of the solid boundary. Temporarily ignoring the no-slip condition, the rate of change of interface circulation at a material point on the solid body is

$$\frac{\mathrm{d}\boldsymbol{\gamma}}{\mathrm{d}t} = \frac{\mathrm{d}\hat{\boldsymbol{n}}}{\mathrm{d}t} \times (\boldsymbol{u} - \boldsymbol{v}) + \hat{\boldsymbol{n}} \times \left[\frac{\mathrm{d}\boldsymbol{u}}{\mathrm{d}t} - \frac{\mathrm{d}\boldsymbol{v}}{\mathrm{d}t} + (\boldsymbol{v} - \boldsymbol{u}) \cdot \nabla \boldsymbol{u} \right]. \qquad (3.10)$$

Terms involving $\boldsymbol{v} - \boldsymbol{u}$ describe the kinematic evolution of interface circulation once it has been created, and are not related to the generation of circulation on a no-slip boundary. Assuming the interface circulation is initially zero, this expression reduces to

$$\frac{\mathrm{d}\boldsymbol{\gamma}}{\mathrm{d}t} = \hat{\boldsymbol{n}} \times \left[\frac{\mathrm{d}\boldsymbol{u}}{\mathrm{d}t} - \frac{\mathrm{d}\boldsymbol{v}}{\mathrm{d}t} \right], \qquad (3.11)$$

and only a relative acceleration between the fluid and the solid generates circulation in the interface. Now, the acceleration of the fluid may be replaced by the tangential momentum equation,

$$\frac{\mathrm{d}\boldsymbol{\gamma}}{\mathrm{d}t} = -\hat{\boldsymbol{n}} \times \left[\nu \nabla \times \boldsymbol{\omega} + \nabla \left(\frac{p}{\rho} + \phi_g \right) + \frac{\mathrm{d}\boldsymbol{v}}{\mathrm{d}t} \right], \qquad (3.12)$$

where ϕ_g is a body force potential. Viscous forces act to maintain the no-slip condition, $\boldsymbol{\gamma} = 0$, and (3.12) can be recast as an expression for the necessary viscous acceleration (boundary vorticity flux),

$$\boldsymbol{\sigma} = \nu \hat{\boldsymbol{n}} \times (\nabla \times \boldsymbol{\omega}) = -\hat{\boldsymbol{n}} \times \left[\nabla \left(\frac{p}{\rho} + \phi_g \right) + \frac{\mathrm{d}\boldsymbol{v}}{\mathrm{d}t} \right]. \qquad (3.13)$$

The right-hand side of (3.13) is the 'inviscid relative acceleration' – the relative acceleration between the fluid and the solid that occurs in the absence of viscous forces. Interface circulation is created during this inviscid acceleration; however, the relative acceleration is opposed by viscous forces, which diffuse vorticity into the fluid via the boundary vorticity flux. Under this interpretation, viscosity is responsible for the diffusion of vorticity, once it is created, but is not involved in the creation of vorticity.

The generation of vorticity on a rotating boundary is easier to interpret if the vorticity field in the solid body is considered. Solid body rotation is represented by the following velocity field:

$$\boldsymbol{v}(\boldsymbol{y}, t) = \boldsymbol{V}(t) + \boldsymbol{\Omega}(t) \times \boldsymbol{y}, \qquad (3.14)$$

where $\boldsymbol{V}$ is the translation velocity, $\boldsymbol{\Omega}$ is the angular velocity and $\boldsymbol{y}$ is the displacement of a material point from the axis of rotation. The corresponding vorticity field is twice the angular velocity, $\nabla \times \boldsymbol{v} = 2\boldsymbol{\Omega}$, and the rate of change of vorticity is

$$\frac{\mathrm{d}}{\mathrm{d}t} \int_{V_s} \nabla \times \boldsymbol{v} \, \mathrm{d}V = \frac{\mathrm{d}}{\mathrm{d}t} \int_{V_s} 2\boldsymbol{\Omega} \, \mathrm{d}V = \frac{\mathrm{d}}{\mathrm{d}t} \left[2\boldsymbol{\Omega} \, \mathrm{Vol}(V_s) \right], \qquad (3.15)$$

where $\mathrm{Vol}(V_s)$ indicates the volume of the solid body, V_s. The solid body contains parallel vortex filaments of equal strength, which are aligned with, and proportional to, the angular velocity vector.

Changes to the angular acceleration of the solid body alter the normal vorticity on the boundary, and the interface circulation generated by this acceleration must satisfy the

generalised solenoidal condition, (3.6). The right-hand-side of (3.13) represents the rate of creation of interface circulation, which satisfies the solenoidal condition in the following manner:

$$\oint_{\partial I} - \left(\hat{\boldsymbol{n}} \times \left[\boldsymbol{\nabla} \left(\frac{p}{\rho} + \phi_g \right) + \frac{\mathrm{d}\boldsymbol{v}}{\mathrm{d}t} \right] \right) \cdot \hat{\boldsymbol{b}} \, \mathrm{d}s = \int_I \boldsymbol{\nabla} \times \left[\boldsymbol{\nabla} \left(\frac{p}{\rho} + \phi_g \right) + \frac{\mathrm{d}\boldsymbol{v}}{\mathrm{d}t} \right] \cdot \mathrm{d}\boldsymbol{S}$$

$$= \int_I 2 \frac{\mathrm{d}\boldsymbol{\Omega}}{\mathrm{d}t} \cdot \mathrm{d}\boldsymbol{S}. \tag{3.16}$$

Here, I is a section of solid boundary, and $\hat{\boldsymbol{b}}$ is the unit normal across the boundary curve, ∂I, which is tangent to the solid boundary. Since $\mathrm{d}/\mathrm{d}t(\mathrm{d}\boldsymbol{S}) = \boldsymbol{\Omega} \times \mathrm{d}\boldsymbol{S}$, the final term in (3.16) is equal to the rate of change of the 'flux of vortex lines' out of the solid body,

$$\frac{\mathrm{d}}{\mathrm{d}t} \int_I 2\boldsymbol{\Omega} \cdot \mathrm{d}\boldsymbol{S} = \int_I 2 \frac{\mathrm{d}\boldsymbol{\Omega}}{\mathrm{d}t} \cdot \mathrm{d}\boldsymbol{S} + \int_I (2\boldsymbol{\Omega}) \cdot (\boldsymbol{\Omega} \times \mathrm{d}\boldsymbol{S}) = \int_I 2 \frac{\mathrm{d}\boldsymbol{\Omega}}{\mathrm{d}t} \cdot \mathrm{d}\boldsymbol{S}. \tag{3.17}$$

In the absence of viscous diffusion, the change in normal vorticity on the solid boundary is balanced by the flux of interface circulation along the boundary (figure 10*a,c*). Only rotational acceleration changes the flux of normal vorticity out of the boundary; translational acceleration $(\mathrm{d}V/\mathrm{d}t)$, pressure gradients (p/ρ) and body forces (ϕ_g) create interface circulation which is solenoidal along the interface, in the sense that

$$\oint_{\partial I} - \left(\hat{\boldsymbol{n}} \times \left[\boldsymbol{\nabla} \left(\frac{p}{\rho} + \phi_g \right) + \frac{\mathrm{d}V}{\mathrm{d}t} \right] \right) \cdot \hat{\boldsymbol{b}} \, \mathrm{d}s = 0. \tag{3.18}$$

Interface circulation is immediately diffused into the fluid, with simultaneous diffusion of normal vorticity along the boundary. Equation (2.2) allows the rate of change of normal vorticity on the fluid side of the boundary to be expressed in terms of the boundary vorticity flux across ∂I,

$$\frac{\mathrm{d}}{\mathrm{d}t} \int_I \boldsymbol{\omega} \cdot \mathrm{d}\boldsymbol{S} = \oint_{\partial I} \left[\nu \hat{\boldsymbol{n}} \times (\boldsymbol{\nabla} \times \boldsymbol{\omega}) \right] \cdot \hat{\boldsymbol{b}} \, \mathrm{d}s = \oint_{\partial I} \boldsymbol{\sigma} \cdot \hat{\boldsymbol{b}} \, \mathrm{d}s. \tag{3.19}$$

By substituting (3.13) into (3.19), and equating the result with (3.16), one obtains

$$\frac{\mathrm{d}}{\mathrm{d}t} \left[\int_I \boldsymbol{\omega} \cdot \mathrm{d}\boldsymbol{S} - \int_I 2\boldsymbol{\Omega} \cdot \mathrm{d}\boldsymbol{S} \right] = 0, \tag{3.20}$$

which demonstrates that the diffusion of normal vorticity along the surface of the solid body due to the generation of tangential vorticity on the interface maintains the condition that vortex lines do not end on the solid boundary. Just as the secondary effect in Lyman's flux maintains the kinematic condition that vortex lines do not end inside the fluid (unless the vorticity is zero), Lyman's flux also provides a natural mechanism to ensure that vortex lines do not end on a no-slip boundary (except if the vorticity is zero).

4. Example flows

Several example flows are examined in this section, demonstrating the advantages afforded by Lyman's definition of the boundary vorticity flux. The flow driven by a rotating sphere is considered first, to illustrate the appearance of normal vorticity on a rotating boundary. Then, flow over a translating sphere is considered. The analysis of vortical structures in the wake is simplified by using Lyman's flux, as key aspects of the wake dynamics, including vortex tilting and viscous cross-annihilation, can be understood by considering the fluxes acting in a two-dimensional reference plane.
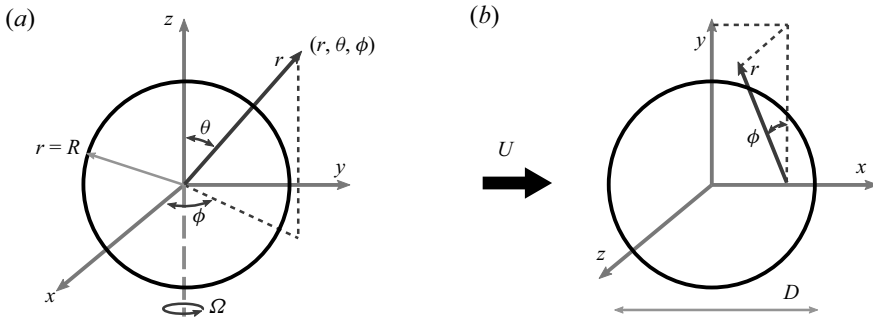
Figure 12. Coordinate system for (*a*) rotating and (*b*) translating sphere flows.

4.1. *Flow over a rotating sphere*

The generation of vorticity on a rotating sphere is investigated in this section. Vortex lines are continuous across the solid boundary, and Lyman's flux clearly illustrates the mechanisms that enforce this condition. The Stokes approximation is considered first, isolating the effects of viscous diffusion. Then, the full Navier–Stokes solution is discussed, where inertial effects generate azimuthal vorticity by vortex tilting in the fluid interior, as well as by tangential pressure gradients and centripetal acceleration at the boundary.

4.1.1. *Stokes flow over a rotating sphere*

By using a Stokes approximation, the generation and diffusion of vorticity are isolated from the effects of advection and vortex tilting. We consider the following transport equations for the 'velocity' field, and its corresponding vorticity field:

$$\frac{\partial \boldsymbol{u}}{\partial t} = -\boldsymbol{\nabla}\left(\frac{p}{\rho}\right) + \nu\nabla^2\boldsymbol{u}, \tag{4.1a}$$

$$\frac{\partial \boldsymbol{\omega}}{\partial t} = \nu\nabla^2\boldsymbol{\omega}. \tag{4.1b}$$

Using the spherical coordinates in figure 12(*a*), the following similarity transformation,

$$u_r(r, \theta, t) = 0, \tag{4.2a}$$

$$u_\theta(r, \theta, t) = 0, \tag{4.2b}$$

$$p(r, \theta, t) = 0, \tag{4.2c}$$

$$u_\phi(r, \theta, t) = \Omega r \sin\theta f(\hat{r}, \tau), \tag{4.2d}$$

$$\hat{r} = r/R, \tag{4.2e}$$

$$\tau = t/(R^2/\nu), \tag{4.2f}$$

reduces (4.1*a*) to a one-dimensional equation

$$\frac{\partial f}{\partial \tau} = \frac{4}{\hat{r}}\frac{\partial f}{\partial \hat{r}} + \frac{\partial^2 f}{\partial \hat{r}^2}. \tag{4.3}$$

Equation (4.3) is solved using a finite-difference method, with two sets of initial and boundary conditions. The first is an impulsively rotated sphere, in an initially stationary

915 A106-22

flow, with

$$f(1, \tau) = 1, \tag{4.4a}$$

$$f(\hat{r}, 0) = 0, \tag{4.4b}$$

while the second is the periodic flow driven by a rotationally oscillating sphere,

$$f(1, \tau) = \sin(\pi k \tau), \tag{4.5a}$$

$$f(\hat{r}, \tau) = f(\hat{r}, \tau + 2/k). \tag{4.5b}$$

The transient Stokes flow driven by the impulsively rotated sphere is illustrated in figure 13. Impulsive rotation of the sphere produces a solid body vorticity field, $\boldsymbol{\omega} = 2\boldsymbol{\Omega}$, inside the sphere. A sheet of interface circulation (velocity discontinuity) is created by the tangential acceleration of the boundary,

$$\boldsymbol{\gamma} = -\Omega R \sin \theta \hat{\boldsymbol{e}}_\theta, \tag{4.6}$$

and the flux of vortex lines out of the solid body is balanced by the flux of circulation along the interface ((3.6)). Effectively, vortex filaments generated during the initial rotation are closed loops, passing through the solid body and continuing along the interface, as illustrated in figure 13(*a*).

The interface circulation is immediately diffused into the fluid by viscous forces, and, for $\tau > 0$, vorticity is non-zero throughout the entire fluid domain. Vortex filaments remain closed loops, passing through the fluid domain, rather than along the interface (figure 13*b*). According to Lyman's flux, the diffusion of tangential vorticity out of the boundary occurs alongside the diffusion of normal vorticity along the boundary, and this ensures that vortex lines are continuous across the interface ((3.20)).

Under Lyman's definition, the boundary vorticity flux is zero for $\tau > 0$, and no new vorticity is created on the boundary. Vorticity in the fluid diffuses away from the sphere, as illustrated in figure 13(*b*–*d*), eventually reaching the following steady-state profile:

$$f(\hat{r}, \infty) = 1/\hat{r}^3, \tag{4.7a}$$

$$\omega_r(\hat{r}, \infty) = 2\Omega \cos \theta / \hat{r}^3, \tag{4.7b}$$

$$\omega_\theta(\hat{r}, \infty) = \Omega \sin \theta / \hat{r}^3. \tag{4.7c}$$

In contrast to unbounded two-dimensional flows, where vorticity continues to diffuse infinitely far from the sphere, vorticity in the present flow is bounded by a $1/\hat{r}^3$ decay with distance from the sphere.

The steady-state behaviour is easily explained by Lyman's flux. The flux of tangential vorticity (ω_θ) in the radial direction (away from the sphere) is

$$\hat{\boldsymbol{e}}_r \cdot \boldsymbol{J} \cdot \hat{\boldsymbol{e}}_\theta = -\nu \frac{\partial \omega_\theta}{\partial r} + \frac{\nu}{r} \frac{\partial \omega_r}{\partial \theta} - \frac{\nu}{r} \omega_\theta. \tag{4.8}$$

On the equator ($z = 0$), the first term is due to gradients in tangential vorticity, while the remaining terms represent the curvature of vortex lines (see § 2.4). Gradients in tangential vorticity act to diffuse vorticity away from the sphere, and this term initially dominates the flow dynamics. However, the curvature of vortex lines acts to diffuse tangential vorticity towards the sphere, and prevents the unbounded diffusion of vorticity away from the sphere. In the steady-state limit, these two effects are exactly balanced, and Lyman's flux is zero throughout the entire fluid region.
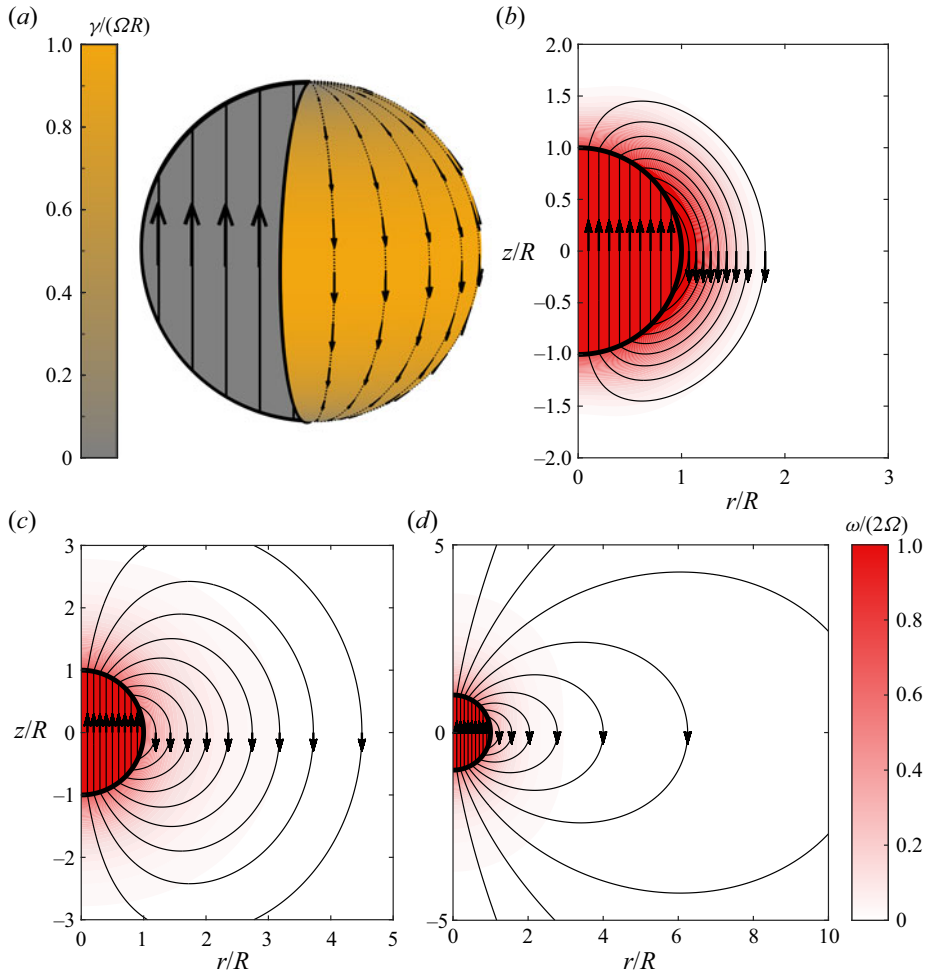
Figure 13. Transient Stokes flow over an impulsively rotated sphere. (*a*) The initial circulation sheet generated during the impulsive acceleration. A cut-away showing vortex lines in the solid body is also provided. (*b–d*) vortex lines in the *r–z* plane, with colour contours of the dimensionless vorticity magnitude, at a dimensionless flow time (*b*) $\tau = 0.05$, (*c*) $\tau = 1$ and (*d*) steady–state flow.

Under Lighthill's definition, however, the flow is more difficult to interpret. The boundary vorticity flux,

$$\sigma_r' = -\nu \frac{\partial \omega_r}{\partial r}, \tag{4.9a}$$

$$\sigma_\theta' = \frac{\partial u_\phi}{\partial t} - \frac{\nu}{r} \frac{\partial \omega_r}{\partial \theta} + \frac{\nu}{r} \omega_\theta, \tag{4.9b}$$

is non-zero for all time, and vorticity is continually generated on the boundary. The boundary vorticity flux depends on vorticity gradients near the boundary, and cannot be determined independently of the vorticity field. Moreover, it is difficult to attribute a distinct vorticity creation mechanism to the vorticity gradient terms.

The steady-state behaviour is also more difficult to interpret under Lighthill's definition. The boundary acts as a constant source of vorticity, and the $1/\hat{r}^3$ profile is a result of

915 A106-24
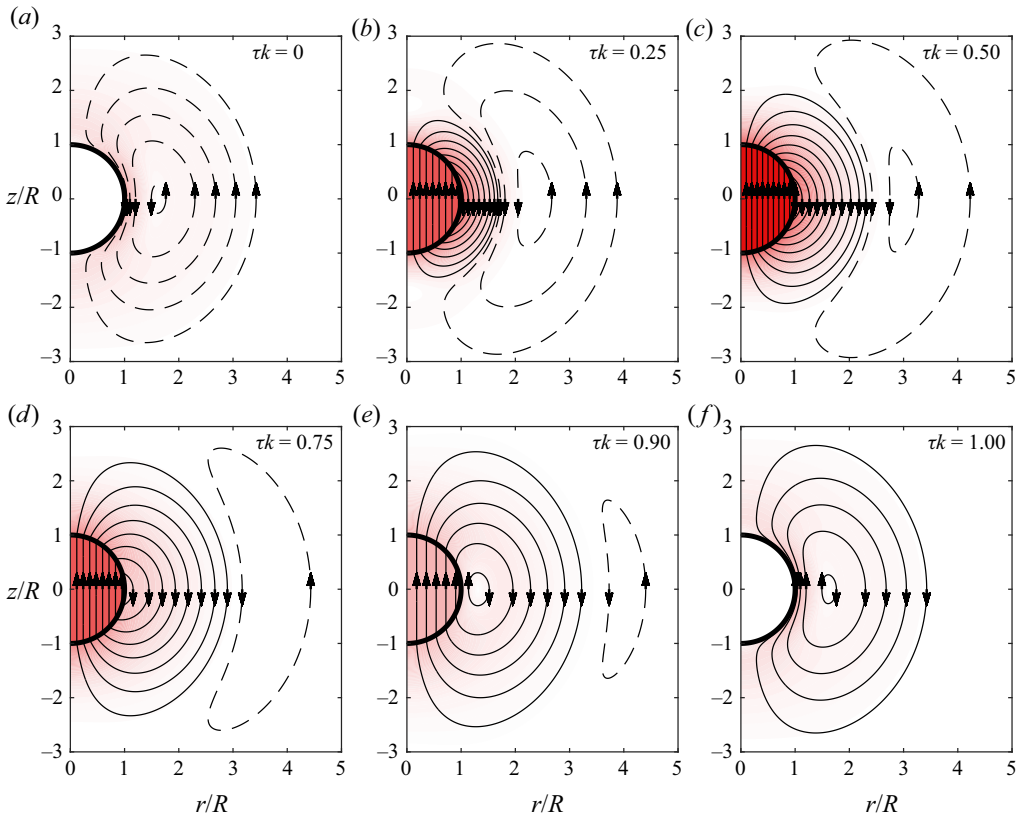
Figure 14. Vortex lines in the *r*–*z* plane, and colour contours of the dimensionless vorticity magnitude, at select time instants during one half-period of transient Stokes flow over an oscillating sphere. The colour map for vorticity contours is the same as for figure 13.

the cross-annihilation of opposite-signed vorticity, as it diffuses away from the sphere. Lyman's definition affords a much simpler interpretation, where no new vorticity is created on the boundary, and the diffusive flux approaches zero in the steady-state.

The impulsively rotated sphere is an example of 'fast generation' (Morton 1984), where all vorticity in the flow is created instantaneously, and the total circulation in both the fluid and the solid remain constant thereafter. The rotationally oscillating sphere, on the other hand, demonstrates 'slow generation', where vorticity is continually generated on the boundary, and the creation and redistribution of vorticity occur simultaneously.

The Stokes flow over a rotationally oscillating sphere, over one half-period of the motion, is presented in figure 14, and a transient animation is also available in supplementary movie 2. Between $k\tau = 0$ and $k\tau = 0.5$, while the sphere is accelerating, the solid-body vorticity in the sphere increases, and closed vortex loops, passing through both the solid and the fluid, are created. While the sphere is decelerating, between $k\tau = 0.5$ and $k\tau = 1$, the solid body vorticity in the sphere decreases and closed vortex loops are shed into the fluid. These flux loops subsequently decay by viscous annihilation, in a manner analogous to the two-dimensional 'O'-point.

The rate of vorticity creation is given by the boundary vorticity flux,

$$\boldsymbol{\sigma}/(\nu\Omega/R) = \pi k \sin\theta \cos(\pi k \tau)\hat{\boldsymbol{e}}_\theta. \qquad (4.10)$$
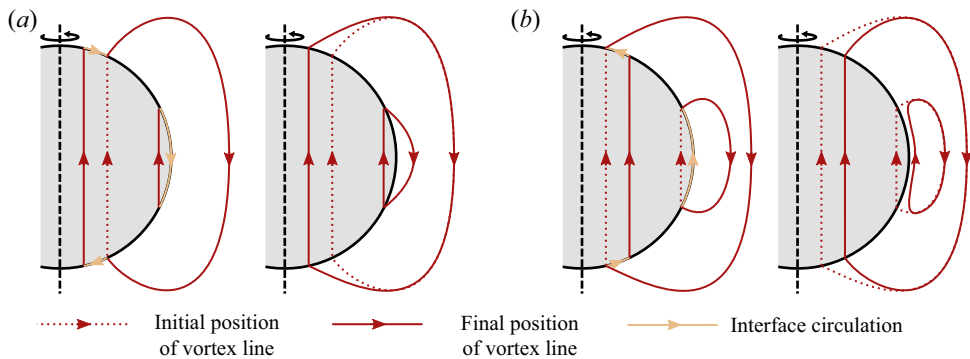
Figure 15. Schematic illustration of the generation and diffusion of vortex lines during (*a*) the acceleration phase, and (*b*) the deceleration phase, for Stokes flow driven by an oscillating sphere. New flux loops are created on the equator during the acceleration phase, while flux loops are shed into the fluid during the deceleration phase.

Positive tangential vorticity, directed from the north pole to the south pole, is generated while the sphere is accelerating, whereas negative tangential vorticity is created while the sphere is decelerating. There is an associated diffusion of normal vorticity – towards the poles during the acceleration phase and towards the equator during the deceleration phase – which ensures that vortex lines are continuous across the boundary.

While the generation and diffusion of vorticity occur simultaneously, the underlying flow behaviour is easier to interpret when these processes are conceptually decoupled. As illustrated in figure 15, the solid body vorticity in the sphere increases (or decreases) during an infinitesimal time interval. The interface circulation created during this time period connects the updated vortex lines in the solid to the vortex lines in the fluid. This circulation is immediately diffused into the fluid, along with the corresponding diffusion of normal vorticity, which ensures that vortex lines remain continuous across the boundary.

This description clearly explains the creation and shedding of flux loops on the equator. During the acceleration phase (figure 15*a*), the interface circulation on the equator connects a new vortex filament in the solid to itself, forming a new flux loop. The interface circulation is immediately diffused into the fluid, and the new vortex loop passes through both the solid and the fluid. During the deceleration phase (figure 15*b*), the interface circulation connects a vortex line in the fluid, which originally passed through the solid, to itself. When the interface circulation is diffused into the fluid, this loop is shed from the sphere and becomes closed entirely within the fluid.

4.1.2. *Inertial flow over a rotating sphere*

The full Navier–Stokes solution to the flow over an impulsively rotated sphere is considered in this section. Inertial effects result in the creation of azimuthal vorticity on the boundary by pressure gradients and centripetal acceleration, as well as by vortex tilting in the fluid interior. Under Lyman's definition, these effects are represented by boundary fluxes, which describe the balance of azimuthal circulation in the r–θ plane. A detailed investigation of this flow has been provided by Calabretto *et al.* (2015) and Calabretto, Denier & Levy (2019), and only details relevant to the azimuthal circulation balance are discussed here.

The numerical results presented in this section were obtained using the commercial finite-volume software ANSYS Fluent, on a 200×200 grid, with axial

symmetry enforced. Adequate numerical resolution was confirmed by running additional simulations on a finer grid (400×400) and with a reduced timestep (from $\Delta t = 1 \times 10^{-3}$ to $\Delta t = 5 \times 10^{-4}$), and changes to both the azimuthal circulation and viscous torque on the sphere, up to $\Omega t = 5$, were below 0.1 %.

The velocity and vorticity fields, at a Reynolds number of $Re = R^2 \Omega / \nu = 1000$, are provided in figure 16, and a transient animation is provided in supplementary movie 3. The initial creation and diffusion of vorticity occurs in a manner similar to the Stokes flow, with the impulsive creation of flux loops, passing through both solid and fluid regions. Following the initial creation of tangential vorticity, positive azimuthal vorticity (ω_ϕ) is continually created on the boundary, while negative azimuthal vorticity is generated by vortex tilting, just outside the boundary layer. The layers of opposite-signed vorticity on the boundary induce a tangential flow (u_θ) towards the equator. The tangential velocity field carries azimuthal vorticity towards the equator, where it encounters opposite-signed azimuthal vorticity from the lower boundary layer. The subsequent boundary layer collision produces a pair of counter-rotating vortices, above and below the equator. The vortex pair induces a radial jet flow, which carries both momentum and vorticity away from the sphere.

The dynamics of azimuthal vorticity can be investigated through a control surface analysis ((2.2)). For the control surface, A, in figure 17(a), the balance of azimuthal circulation is

$$\frac{\mathrm{d}\Gamma_\phi}{\mathrm{d}t} = \frac{\mathrm{d}}{\mathrm{d}t}\left(\int_A \omega_\phi \, dA\right) = F_{vt.} + F_{dcy.} + F_{gen.}, \tag{4.11a}$$

$$F_{vt.} = \int_{eqt.} -u_\phi \omega_z \, \mathrm{d}x + \int_{sph.} -u_\phi (\hat{\boldsymbol{n}} \cdot \boldsymbol{\omega}) \, \mathrm{d}s, \tag{4.11b}$$

$$F_{dcy.} = \int_{eqt.} -\nu \frac{\partial \omega_\phi}{\partial z} \, \mathrm{d}x + \int_{ax.} -2\nu \frac{\partial \omega_\phi}{\partial x} \, \mathrm{d}z, \tag{4.11c}$$

$$F_{gen.} = \int_{sph.} \hat{\boldsymbol{n}} \times (\boldsymbol{\nabla} \times \boldsymbol{\omega}) \, \mathrm{d}s. \tag{4.11d}$$

The boundaries of A are: *sph.*, the surface of the sphere; *eqt.*, the equatorial axis ($z = 0$); and *ax.*, the symmetry axis ($x = 0$). The contributions to the total azimuthal circulation include the effects of vortex tilting ($F_{vt.}$), viscous annihilation on the equatorial and symmetry axes ($F_{dcy.}$) and the creation of vorticity on the solid boundary ($F_{gen.}$).

The time history of Γ_ϕ, as well as the contributions to the circulation balance from each of the boundary fluxes, is provided in figure 18. The azimuthal circulation in A is negative, and the magnitude of negative circulation increases throughout the time period considered. The circulation balance is dominated by the creation of negative circulation by vortex tilting ($F_{vt.}$), which is stronger than the generation of positive circulation on the boundary ($F_{gen.}$). The intensity of vortex tilting increases during the boundary layer collision ($\tau \approx 5$), with the largest rate-of-change of circulation occurring during this collision. The viscous annihilation of vorticity ($F_{dcy.}$) is only significant after the boundary layer collision, as opposite-signed vorticities from the upper and lower vortices cross-annihilate on the equatorial axis.

While the effects of vortex tilting are represented as a boundary flux ($F_{vt.}$), vortex tilting is usually considered to be a local effect occurring in the fluid interior (Kolár 2003). Referring to the sketch in figure 17(b), the boundary fluxes in $F_{vt.}$ ((4.11b)) represent the rate of advection of vortex lines in the azimuthal direction, across the outer boundary of A
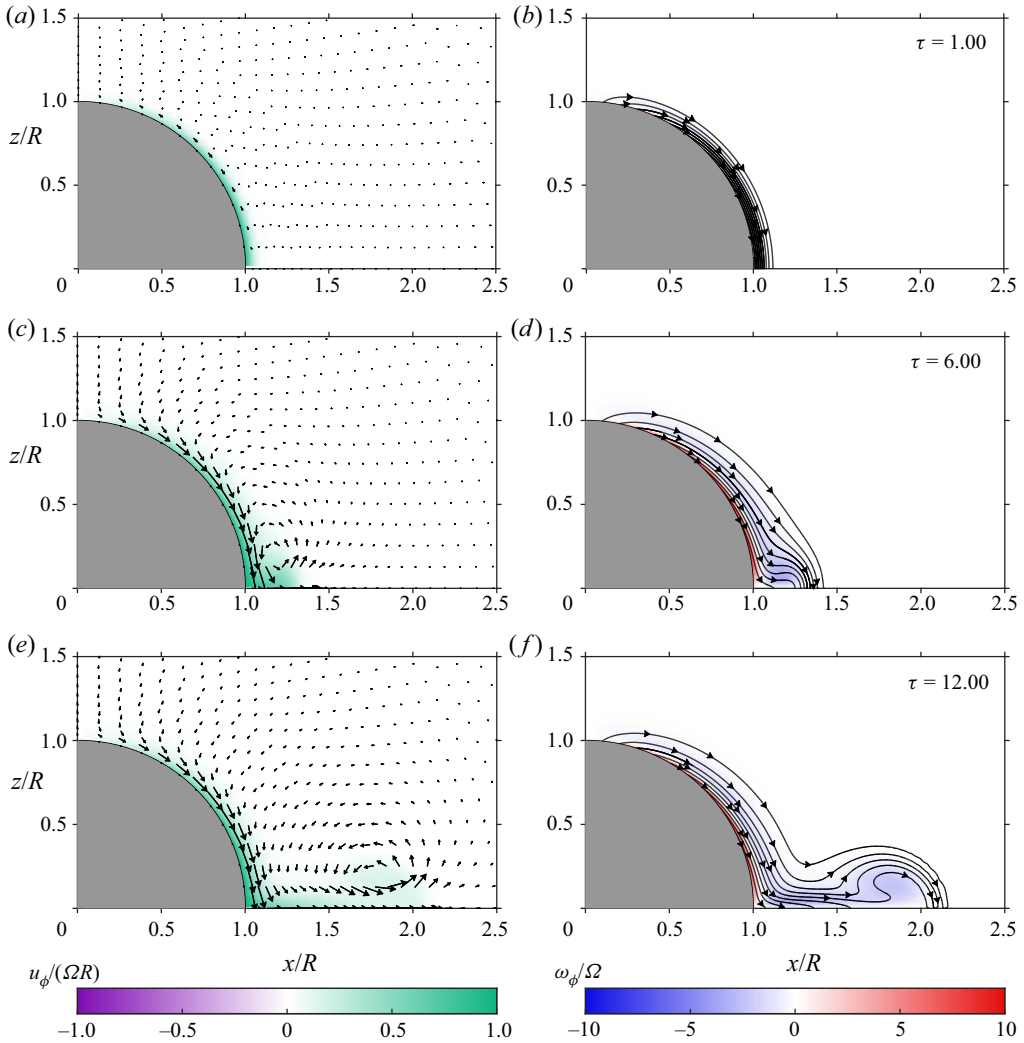
Figure 16. Contours of azimuthal velocity (a,c,e), and azimuthal vorticity (b,d,f), as well as a vector plot of the in-plane velocity (a,c,e), and the projection of vortex lines in the x–z plane, computed as contours of constant $\xi = 2\pi x u_\phi$ (b,d,f). Visualisations are provided at a range of dimensionless flow-times, $\tau = \Omega t$. Velocity vectors are displayed on a coarse grid, and are not representative of the mesh used for numerical simulation.

(see § 2.2). Each vortex line enters A through the boundary of the sphere and exits along the equatorial plane. The negative value of F_{vt} indicates that the rate of transport along the sphere is greater than the rate of transport along the equator, so that the flux of vortex lines (negative azimuthal circulation) in A must be increasing.

An expression for the boundary vorticity flux is obtained from (3.13):

$$\boldsymbol{\sigma} = \frac{\partial u_\phi}{\partial t}\boldsymbol{e}_\theta + \left[\frac{u_\phi^2}{R\tan\theta} - \frac{1}{\rho R}\frac{\partial p}{\partial\theta}\right]\boldsymbol{e}_\phi. \tag{4.12}$$

The first term describes the impulsive creation of tangential vorticity during the initial rotation of the sphere. The remaining two terms describe the continuous generation of

915 A106-28
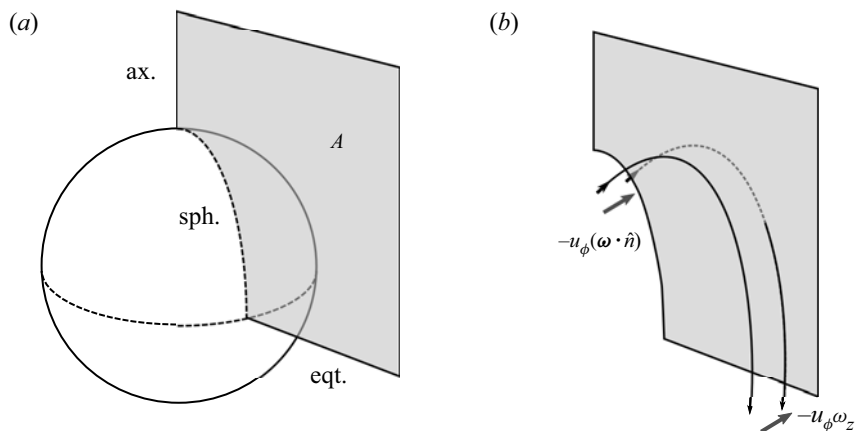
Figure 17. (*a*) The control surface A, used to compute the total azimuthal circulation in (4.11*a*). (*b*) Illustration of the various terms in F_{vt}. Each vortex line enters A through the sphere, and leaves along the equatorial axis. The generation of negative azimuthal vorticity by vortex tilting is related to the condition that the rate of advection of vortex lines across A, in the azimuthal direction, is greater on the sphere than on the equatorial axis.
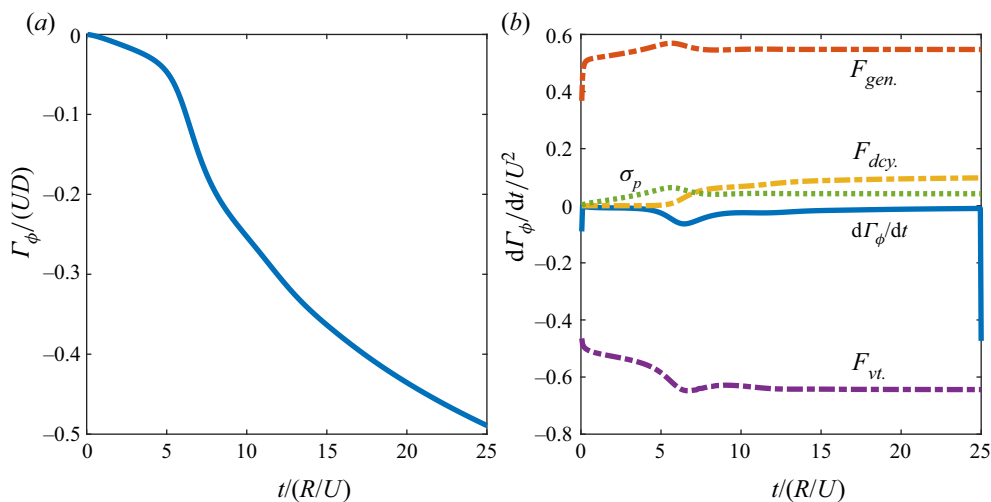

Figure 18. (*a*) Time history of azimuthal circulation in the upper quadrant of the x–z plane, and (*b*) contributions of each flux term in (4.11*a*) to the total circulation balance: $F_{vt.}$, the effects of vortex tilting; $F_{gen.}$, the generation of vorticity on the surface of the sphere; and $F_{dcy.}$, the decay of vorticity due to viscous cross-annihilation. σ_p is the contribution of pressure gradients to $F_{gen.}$.

azimuthal vorticity, by pressure gradients ($\partial p / \partial \theta$) and centripetal acceleration (u_ϕ^2 / R). From figure 18, pressure gradients (σ_p) provide only a small contribution to the boundary vorticity flux, and most of the azimuthal circulation is created by the centripetal acceleration. Points on the solid body undergo circular motion, with a (tangential component of) centripetal acceleration equal to $u_\phi^2 / (R \tan \theta)$. In the absence of viscous forces, boundary fluid elements would suffer a centrifugal acceleration towards the equator, generating azimuthal circulation in the interface. Circulation generated in this

manner is immediately diffused into the fluid by the viscous forces which enforce the no-slip condition.

The dynamics of azimuthal vorticity has been expressed as a two-dimensional conservation law ((4.11a)), using Lyman's definition of the boundary vorticity flux. Under Lighthill's definition, azimuthal vorticity may diffuse in the out-of-plane direction, requiring a fully three-dimensional description. Owing to axial symmetry, azimuthal vorticity is essentially a two-dimensional field, and the two-dimensional description afforded by Lyman's flux is clearly a more convenient representation.

4.2. *Flow over a translating sphere*

Flow over a translating sphere is examined in this section. Lyman's flux provides a more convenient description of vorticity creation, as the boundary flux can be computed directly from the surface pressure distribution. Moreover, Lyman's flux provides a powerful description of three-dimensional wake dynamics, where the evolution of vortical structures in the wake can be understood by considering the fluxes of vorticity in the two-dimensional symmetry plane.

The flow over a sphere has been extensively studied, and a comprehensive review is provided by Tiwari *et al.* (2020). Three Reynolds numbers are considered here, $Re = UD/\nu = 125$, 250 and 300, corresponding to the first three wake modes: the axisymmetric regime ($20 < Re < 210$), the steady planar symmetric mode ($210 < Re < 270$) and the symmetric vortex shedding regime ($270 < Re < 800$). These wake modes have previously been discussed in detail by Johnson & Patel (1999).

The results presented in this section were obtained numerically, using the commercial finite-volume software ANSYS Fluent. These results display both qualitative and quantitative agreement with Johnson & Patel (1999), and adequate grid resolution was confirmed by running simulations with two separate grid resolutions ($\approx 4 \times 10^4$ and $\approx 3 \times 10^5$ elements, on a two-dimensional mesh, were used for the $Re = 125$ flow; $\approx 2 \times 10^6$ and $\approx 9 \times 10^6$ elements were used for the $Re = 250$ case). In each case, the lift and drag coefficients were found to vary by less than 1.8 % between the coarse and fine grids. The transient simulation at $Re = 300$ was performed on the $\approx 2 \times 10^6$ element grid.

4.2.1. *Axisymmetric wake mode – $Re = 125$*

The axisymmetric wake mode occurs for Reynolds numbers below $Re = 210$. Referring to the cylindrical coordinate system in figure 12(b), velocity vectors are confined to the r–x plane, and the only non-zero vorticity component is the azimuthal vorticity, ω_ϕ. The steady-state vorticity field, along with velocity streamlines, is provided in figure 19, at $Re = 125$. Negative vorticity is created near the front of the sphere and is transported downstream by advection. A small quantity of positive vorticity is generated behind the sphere; however, it is almost immediately eliminated by cross-annihilation with the surrounding negative vorticity. The intensity of vorticity in the wake decreases downstream of the sphere, due to the cross-annihilation of opposite-signed vorticities from each side of the symmetry axis. The cross annihilation process is analogous to that at a two-dimensional 'O-'point (§ 2.3), as vortex lines are closed loops orbiting the symmetry axis.

For the present flow, Lyman's flux allows the vorticity creation rate to be determined directly from the surface pressure isobars: $\boldsymbol{\sigma}$ is aligned in the direction of the isobars and is proportional to the pressure gradient. As illustrated in figure 20, surface isobars,
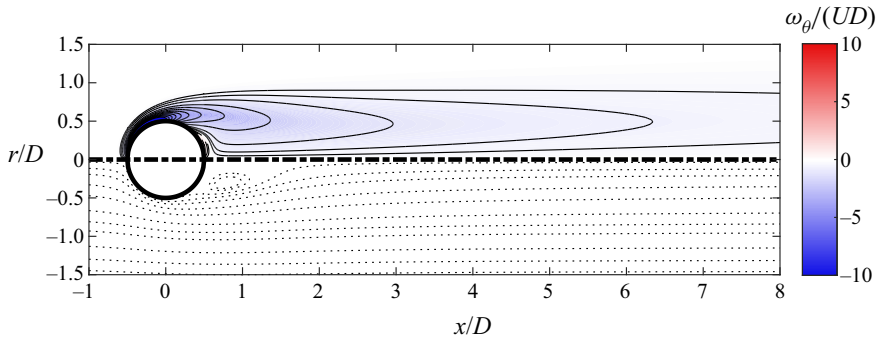
Figure 19. Contour plot of azimuthal vorticity (top) and streamlines (bottom) for steady flow over a sphere at $Re = 125$.
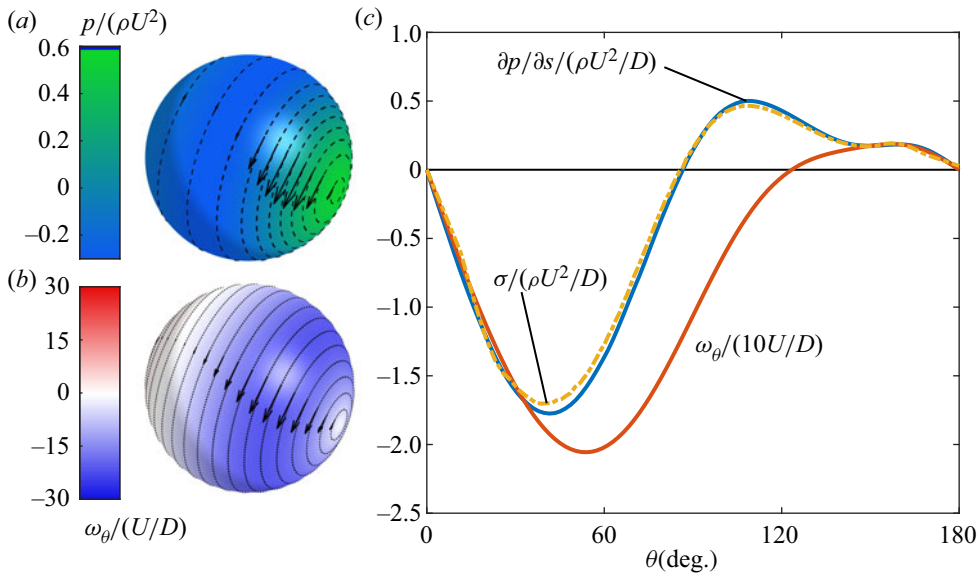

Figure 20. Contour plots of (a) surface pressure, and (b) boundary vorticity magnitude, on the surface of the sphere, at $Re = 125$. Vectors indicate (a) the boundary vorticity flux, and (b) the boundary vorticity, along with representative vorticity lines on the surface. (c) gives the distributions of boundary vorticity, and boundary vorticity flux, on the surface of the sphere, where $\theta = \sin^{-1}(-r/x)$ is the polar angle.

and hence the boundary vorticity flux, are aligned in the azimuthal direction, and only azimuthal vorticity is created on the boundary. The strong negative pressure gradient near the front of the sphere produces a strong flux of negative vorticity in this region, while a weaker flux of positive vorticity occurs in the adverse pressure gradient behind the sphere. Corresponding trends are observed in the boundary vorticity profile (figure 20b), where intense negative vorticity is located near the front of the sphere and weak positive vorticity is located at the rear.

Lyman's flux also describes the transport of azimuthal vorticity, ω_ϕ, in terms of fluxes acting in the r–x plane. Referring to figure 21(a), the net flux of vorticity in the streamwise direction is denoted $F_x(x)$. As flow is steady, the net flux into any closed control volume is zero, and the variation in $F_x(x)$ in the streamwise direction is balanced by either the
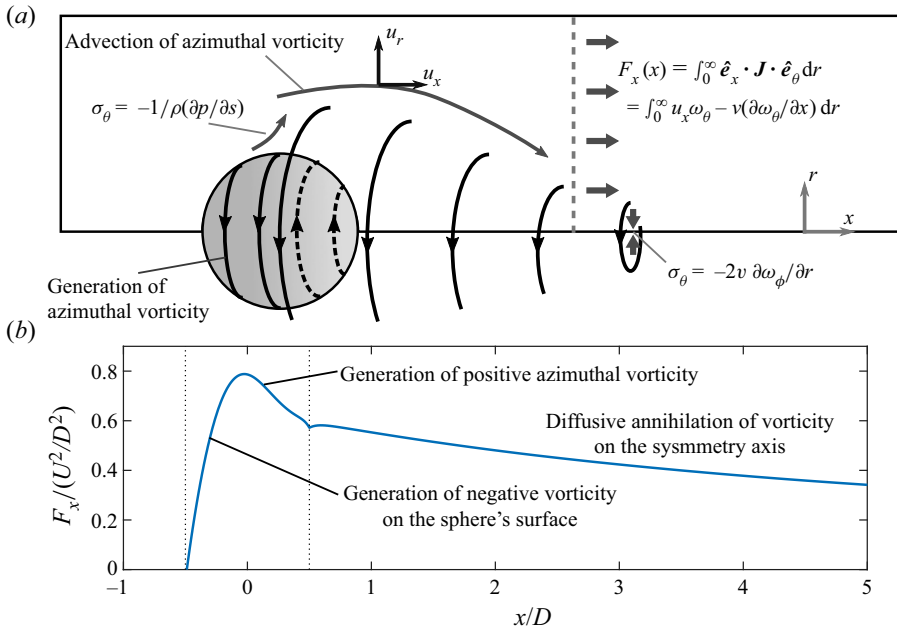
915 A106-31

Figure 21. (*a*) A schematic illustration of vorticity transport in the *x*–*r* plane. $F_x(x)$ is the net flux of ω_ϕ in the streamwise direction, while σ_ϕ gives the rate of generation of vorticity on the sphere, and the rate of viscous annihilation on the symmetry axis. (*b*) The streamwise distribution of streamwise vorticity flux, $F_x(x)$.

creation of vorticity on the sphere or the viscous annihilation of vorticity on the symmetry axis.

The streamwise distribution of $F_x(x)$ is plotted in figure 21(*b*). Over the surface of the sphere ($|x|/D < 0.5$), gradients in F_x are due to the boundary vorticity flux,

$$\frac{\mathrm{d}F_x}{\mathrm{d}x} = [\hat{\boldsymbol{n}} \times (\boldsymbol{\nabla} \times \boldsymbol{\omega})] \cdot \hat{\boldsymbol{e}}_\phi \frac{\partial s}{\partial x} = \frac{1}{\rho}\frac{\partial p_s}{\partial s}\frac{\partial s}{\partial x} = \frac{1}{\rho}\frac{\partial p_s}{\partial x}, \tag{4.13}$$

where s is an arc-length parametrisation of the sphere, and p_s is the pressure on the surface. The generation of negative vorticity at the front of the sphere increases F_x, while the generation of positive vorticity behind the sphere produces a small decrease in F_x.

When $|x|/D > 0.5$, the variation in F_x is due to the viscous cross-annihilation of vorticity on the symmetry axis. The flux of vorticity across the symmetry axis is

$$\frac{\mathrm{d}F_x}{\mathrm{d}x} = -2\nu \frac{\partial \omega_\theta}{\partial r}, \tag{4.14}$$

which acts to decrease the streamwise vorticity flux downstream of the sphere, as vortex loops are annihilated by cross-diffusion on the symmetry axis. Analogous to the annihilation of flux at a two-dimensional 'O'-point, opposite-signed vorticities from above and below the symmetry plane are cross-annihilated, reducing the total circulation orbiting the symmetry axis.

The analysis in this section demonstrates two advantages of Lyman's definition of the vorticity flux. First, the vorticity creation rate on a solid boundary can be determined directly from the distribution of surface pressure. Second, Lyman's definition is easily applied to curvilinear coordinate systems, by using the surface-integral formulation of the vorticity transport equation. This allows, for example, a direct measure of the viscous annihilation of vortex loops, which is not readily afforded by Lighthill's definition.
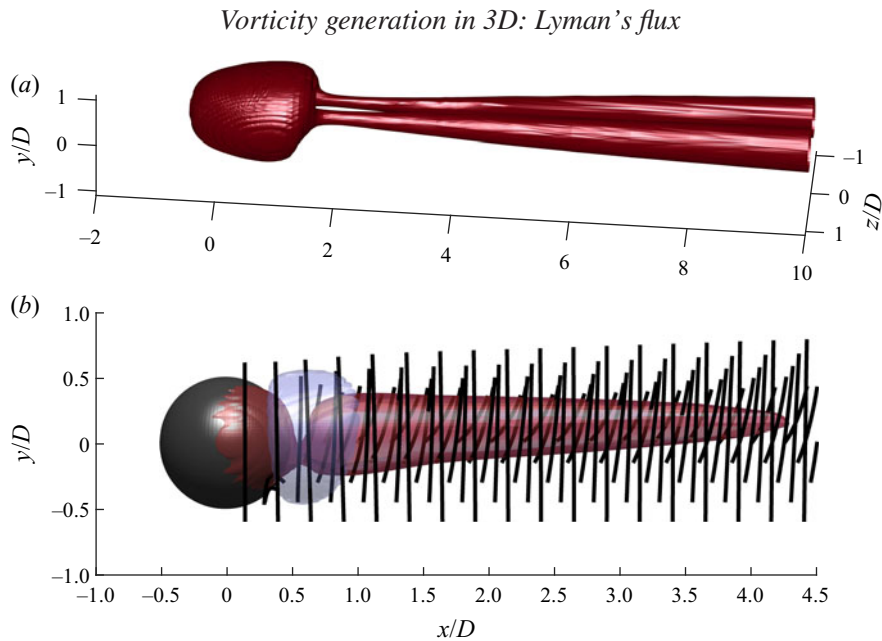
Figure 22. (*a*) Two streamwise-oriented vortices in the wake behind a sphere at $Re = 250$, visualised using the λ_2 criterion. (*b*) Isosurfaces of streamwise vorticity: $\omega_x/(U/D) = 0.3$ (red), and $\omega_x/(U/D) = -0.1$ (blue), as well as representative vortex lines.

4.2.2. *Planar steady wake* – $Re = 250$

The planar steady wake mode occurs at Reynolds numbers in the range $210 < Re < 270$. As illustrated in figure 22(*a*), the dominant wake structure is a pair of streamwise-oriented vortices. These structures are visualised using the λ_2 criterion (Jeong & Hussain 1995), consistent with previous numerical studies (Johnson & Patel 1999; Gushchin *et al.* 2002; Gushchin & Matyushin 2006). While the λ_2 criterion is used to visualise vortical structures in the wake, the full vorticity field must be considered when interpreting the dynamical evolution of these structures (Bernard 2011, 2019). By using Lyman's definition of the vorticity flux, key aspects of the wake dynamics can be understood by considering the vorticity fluxes in the two-dimensional symmetry plane.

The vortices in figure 22(*a*) are essentially composed of streamwise vorticity (Thompson, Leweke & Provansal 2001), as illustrated in figure 22(*b*). The left-hand ($z > 0$) vortex contains positive streamwise vorticity, while the right-hand vortex contains negative vorticity. The outer-wake region also contains some streamwise vorticity, of opposite sign to the main vortex. While some streamwise vorticity is created on the sphere, most of the streamwise vorticity in the wake is created by the tilting of spanwise vorticity (ω_y or ω_z). In figure 22(*b*), vorticity loops shed from the sphere become tilted in the near-wake region, and the streamwise component of vorticity in these loops is responsible for the streamwise vortices (Thompson *et al.* 2001).

Vortex lines near the sphere in figure 22(*b*) are nearly vertical, indicating that the generation of spanwise-oriented vorticity (ω_y, ω_z) is much stronger than the generation of streamwise vorticity. The pressure contours and vortex lines plotted in figure 23(*a,b*) show that near the front of the sphere, the pressure field is nearly axisymmetric. This is the region with the strongest pressure gradients, and where most of the vorticity in the wake is generated. Thus, most of the vortex loops that separate from the surface of the sphere are initially aligned nearly perpendicular to the flow direction and contain little
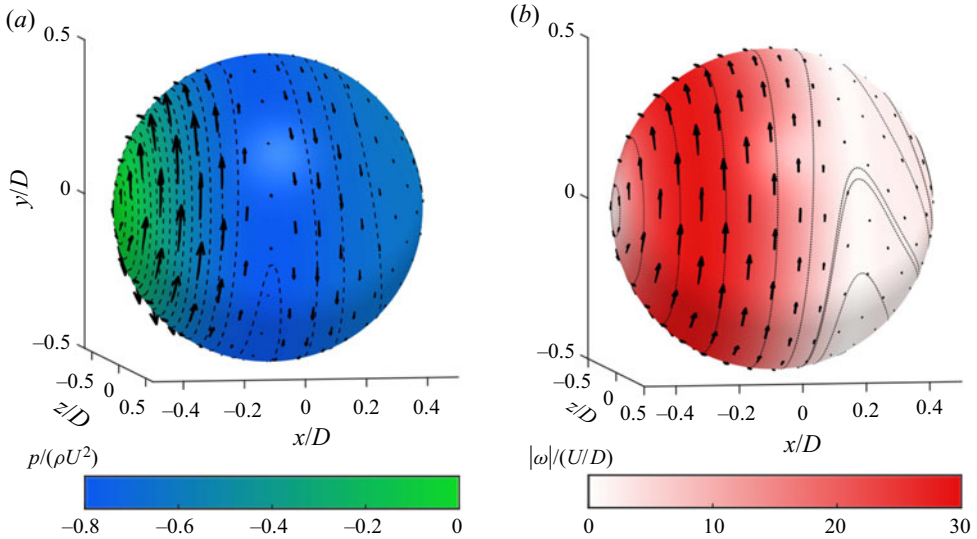
Figure 23. Colour contours of (*a*) surface pressure, and (*b*) vorticity magnitude. Pressure isobars are plotted in (*a*), while surface vortex lines are included in (*b*). Vectors in (*a*,*b*) are of the boundary vorticity flux (σ) and vorticity (ω), respectively.
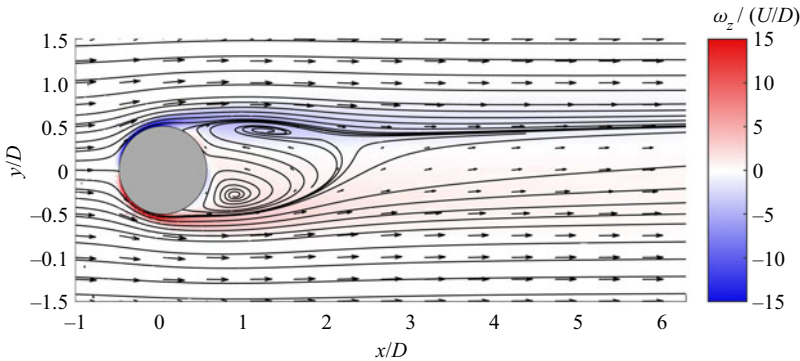

Figure 24. Colour contours of spanwise-oriented vorticity, ω_z, as well as a vector plot and streamlines of the velocity field, in the symmetry plane ($z = 0$), for flow past a sphere at $Re = 250$.

streamwise vorticity. However, the pressure field at the rear of the sphere shows clear loss of axial symmetry. Pressure contours are tilted, and some streamwise vorticity is generated behind the sphere. Surface vortex lines behind the sphere are also tilted, and there is some streamwise vorticity, concentrated towards the rear surface of the sphere.

A contour plot of vorticity in the symmetry plane, along with streamlines and velocity vectors, is presented in figure 24. The recirculation region is not symmetric, with the lower recirculation region being larger, and closer to the sphere. The lower recirculation entrains vorticity into the near wake to a greater extent than the upper recirculation, and the recirculating region behind the sphere contains a greater quantity of positive vorticity.

Using Lyman's flux, many important aspects of the three-dimensional wake dynamics can be understood by considering the fluxes of vorticity in the symmetry plane. The net flux of spanwise vorticity (ω_z) in the downstream direction, $F_x(x)$, is defined in precisely

915 A106-34

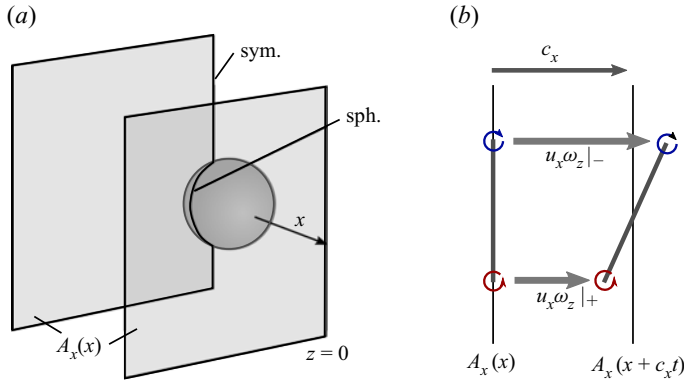(*a*)   (*b*)

Figure 25. (*a*) Reference surface, A_x, for computing the total streamwise circulation in each vortex. In the wake, only fluxes across the symmetry plane boundary ($z = 0$) contribute to the vorticity balance. When $-0.5 < x/D < 0.5$, the circulation balance includes fluxes across the symmetry plane, and across the surface of the sphere. (*b*) Schematic illustration of (4.18), when $F_x^* < 0$. The rate of transfer of the upper portion of vortex loops through A_x exceeds the rate of transfer of the lower portion, indicating the tilting of vortex lines and the generation of streamwise vorticity.

the manner done for axisymmetric flow:

$$F_x(x) = \int_{-\infty}^{\infty} \left[u_x \omega_z - \nu \left(\frac{\partial \omega_z}{\partial x} - \frac{\partial \omega_x}{\partial z} \right) \right] \, \mathrm{d}y. \tag{4.15}$$

As flow is steady, F_x is zero at each streamwise location. However, opposing contributions to F_x from regions of positive (F_x^+) and negative (F_x^-) vorticity decrease in the spanwise direction, due to the viscous cross-annihilation of opposite-signed vorticities on the line $\omega_z = 0$,

$$\frac{\partial F_x^+}{\partial x} = -\frac{\partial F_x^-}{\partial x} = \nu \left(\frac{\partial \omega_z}{\partial y} - \frac{\partial \omega_y}{\partial z} \right) \Bigg|_{\omega_z = 0}. \tag{4.16}$$

As in the axisymmetric wake, this represents the viscous annihilation of closed vortex loops, and Lyman's flux provides a direct measure of the rate of annihilation. The general trends in both F_x^- and F_x^+ are the same as for the axisymmetric flow and are not repeated here.

The generation of streamwise vorticity by vortex tilting can also be described by vorticity fluxes in the symmetry plane. Consider the reference surface, $A_x(x)$, in figure 25(*a*), which is orthogonal to the streamwise direction and comprises the semi-infinite plane $z \geq 0$. The streamwise circulation in A_x,

$$I_{\omega_x} = \int_{A_x} \omega_x \, \mathrm{d}A, \tag{4.17}$$

which is plotted in figure 26(*a*), indicates the strength of the streamwise vortices at each streamwise location. I_{ω_x} increases slightly between $x/D = -0.5$ and $x/D = 0.5$, due to creation of vorticity on the sphere's surface. The sharp rise in I_{ω_x} behind the sphere is due to vortex tilting in the near-wake region, and the gradual decay of I_{ω_x} in the wake is due to the viscous cross-annihilation of streamwise vorticity on the symmetry plane.
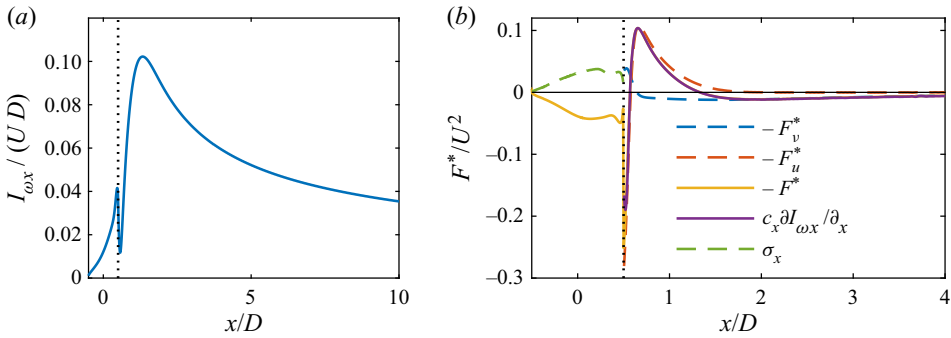
Figure 26. The streamwise distribution of (*a*) the streamwise circulation, I_{ω_x}, and (*b*) the vortex tilting fluxes, F_x^*. The vertical dotted line indicates the maximum downstream extent of the sphere. Various terms in (4.20) are illustrated for $|x|/D < 0.5$, while the balance of fluxes in (4.18) are provided for $x/D > 0.5$, including the contributions to F_x^* from both viscous (F_v^*) and advective (F_u^*) effects.

As flow is steady, the rate of change of I_{ω_x} in a stationary surface is zero. Instead, the rate of change of circulation in a surface travelling downstream is considered,

$$\frac{\mathrm{d}}{\mathrm{d}t}\left(I_{\omega_x}(x + c_x t)\right) = c_x \frac{\mathrm{d}I_{\omega_x}}{\mathrm{d}x} = -\int_{-\infty}^{\infty}\left[(u_x - c_x)\omega_z - \nu\left(\frac{\partial \omega_z}{\partial x} - \frac{\partial \omega_x}{\partial z}\right)\right]\mathrm{d}y = -F_x^*, \tag{4.18}$$

where c_x is a mean advection velocity, weighted by the spanwise vorticity magnitude,

$$c_x = \int_{-\infty}^{\infty} u_x |\omega_z| \,\mathrm{d}y / \int_{-\infty}^{\infty} |\omega_z| \,\mathrm{d}y. \tag{4.19}$$

Equation (4.18) has a simple physical interpretation. F_x^* is the net flux of spanwise vorticity in the streamwise direction, computed in a reference frame travelling downstream with velocity c_x. When $F_x^* < 0$, negative spanwise vorticity is transported downstream of $x + c_x t$ more rapidly than positive spanwise vorticity. As illustrated in figure 25(*b*), this causes vortex loops to become tilted in the downstream direction, generating streamwise vorticity. Of course, equal quantities of opposite-signed streamwise vorticity are created on each side of the symmetry plane, and no net creation of vorticity occurs.

The distribution of F_x^* with streamwise location is presented in figure 26(*b*). In order to capture the balance between the generation of streamwise vorticity on the sphere and the downstream transport, we have used $c_x = 0$ between $x/D = -0.5$ and $x/D = 0.5$. The balance of streamwise vorticity reduces to

$$\frac{\mathrm{d}I_{\omega_x}}{\mathrm{d}t} = -\int_{symm}\left[u_x\omega_z - \nu\left(\frac{\partial \omega_z}{\partial x} - \frac{\partial \omega_x}{\partial z}\right)\right]\mathrm{d}y + \int_{sphere}\sigma_x\,\mathrm{d}y = 0, \tag{4.20}$$

and the generation of streamwise vorticity on the solid boundary is exactly balanced by the transport fluxes, which include the effects of diffusion, advection and vortex tilting.

For $x/D > 0.5$, F_x^* gives the rate of change of I_{ω_x}, according to (4.18). The contributions to F_x^* from advection (F_u) and viscosity (F_v) are also indicated in figure 26(*a*). Vortex tilting, which is associated with the advective fluxes, is responsible for most of the streamwise vorticity in the wake. Vortex tilting is strongest in the near-wake region, between $x/D = 0.5$ and $x/D = 2$, which suggests that the formation of streamwise vortices can be attributed to the recirculation region in the near wake. For $x/D > 2$, F_x^* is almost entirely due to viscous fluxes, which reduce the magnitude of streamwise vorticity as opposite-signed vorticities from each vortex are cross-annihilated on the symmetry plane.

915 A106-36

By using Lyman's definition of the boundary vorticity flux, vorticity transport has been expressed in terms of fluxes acting in the symmetry plane, affording an elegant description of the wake dynamics. Tangential pressure gradients on the surface of the sphere generate closed vorticity loops, which are nearly perpendicular to the free-stream flow. These vorticity loops are carried downstream by advection; however, the lower portion of these loops are entrained into the recirculation region to a greater extent than the upper portions (figure 24), and are impeded from travelling downstream. As a result, vortex lines become tilted in the streamwise direction (figure 25), generating the streamwise vorticity which comprise the wake vortices.

4.2.3. *Vortex shedding mode – Re = 300*

The wake becomes unsteady above $Re = 270$, and, by $Re = 300$, transitions to the vortex shedding mode. As illustrated in figure 27(*a*), alternately-oriented hairpin vortices are periodically shed from the sphere. The isosurfaces of streamwise (*b*) and spanwise (*c*) vorticity, shown in figure 27, reveal that the vortex heads are regions of concentrated spanwise vorticity (ω_z), while the vortex legs are regions of counter-rotating streamwise vorticity (ω_x). The heads of the upper vortices comprise negative spanwise vorticity, while the lower vortex heads contain positive spanwise vorticity. The legs of the upper vortices comprise spanwise vorticity from the inner wake, which is positive for $z > 0$ and negative for $z < 0$. The legs of the lower vortices contain spanwise vorticity from the outer wake, which is of opposite orientation to the upper vortices.

The vortex formation process in the near wake can be interpreted by considering the dynamics of vorticity in the symmetry plane. Streamlines and vorticity contours are provided in figure 28, along with streamwise distributions of the mean spanwise vorticity,

$$I_{\omega_z} = \int_{y=-\infty}^{y=\infty} \omega_z \, \mathrm{d}y, \tag{4.21}$$

vorticity transport (F_x) and vortex tilting (F_x^*) fluxes. The upper vortices, $P1$ and $P2$, are identified as regions of elevated negative I_{ω_x}, while the lower vortices, $S1$ and $S2$, are concentrations of positive I_{ω_x}.

The upper vortices form from the periodic shedding of the upper recirculation bubble. At $\phi = 0$, a new recirculation, $P2$, is beginning to form, while $P1$ has been shed into the wake. Between $\phi = 0$ and $\phi = \pi$, $P2$ remains attached to the sphere and grows in magnitude. During this process, F_x is negative upstream of $P2$ and positive downstream of $P2$ (figure 28*b*), indicating that negative vorticity is rapidly drawn into $P2$ from upstream, and accumulates inside the recirculation region. By $\phi = 3\pi/2$, $P2$ is shed into the wake. F_x is approximately proportional to I_{ω_z}, indicating the advection of $P2$ downstream, rather than the accumulation of vorticity in the vortex head.

While $P2$ is developing, between $\phi = 0$ and $\phi = \pi$, a concentration of positive vorticity, $S1$, is shed into the wake. This appears to be due to reduced intake of positive vorticity into the lower recirculation bubble, producing a weaker recirculation region and an elevated concentration of spanwise vorticity in the outer wake. This is consistent with the observation that the legs of the lower vortices are formed from outer-wake vorticity.

The vortex lines in figure 27(*b*) demonstrate that vortex formation is associated with the alternate tilting of vortex loops in the upstream and downstream directions. As illustrated in figure 29, during the formation of the upper vortex head, the elevated flux of negative vorticity tilts vortex loops forwards, generating positive streamwise vorticity (the legs of the upper vortex). Similarly, vortex loops are tilted in the opposite direction during the formation of the lower vortices, creating negative streamwise vorticity. This is supported
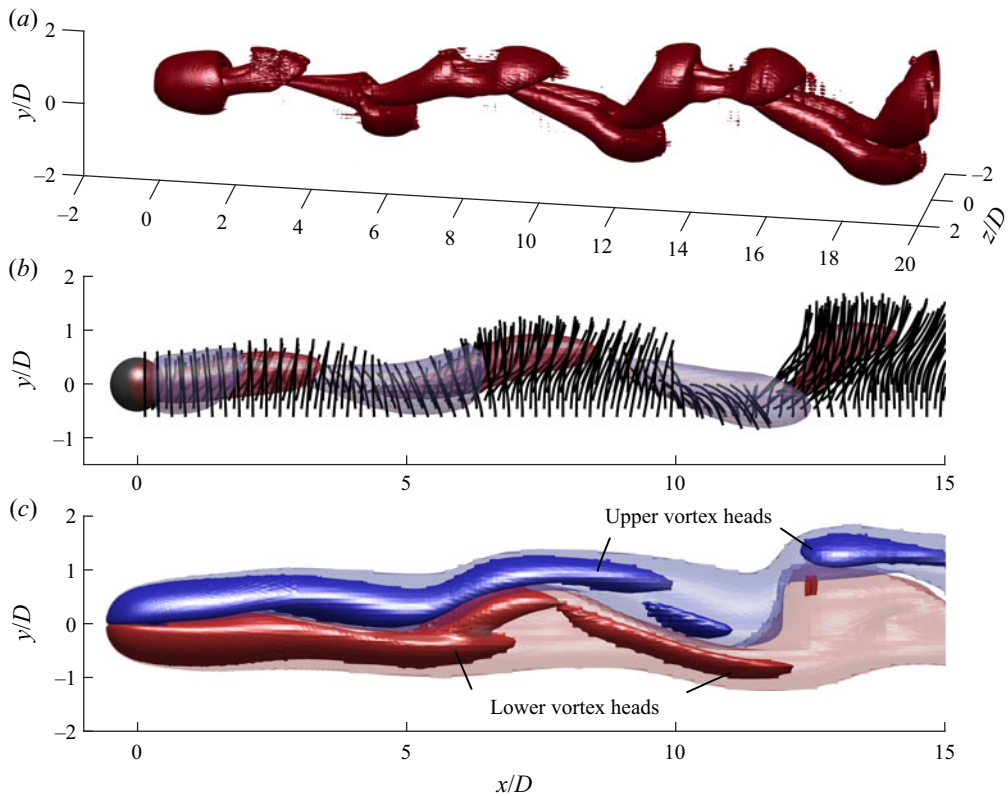
Figure 27. Instantaneous visualisations of the wake behind a sphere at $Re = 300$. (*a*) Isosurfaces of $\lambda_2 = 0$, (*b*) Isosurfaces of streamwise vorticity, as well as representative vortex lines, and (*c*) isosurfaces of spanwise vorticity (ω_z). Opaque isosurfaces in (*c*) correspond to $\omega_z/(UD) = \pm 0.3$, while transparent isosurfaces are for $\omega_z/UD = \pm 0.05$.

by the vortex tilting fluxes, F_x^* (figure 28), which demonstrate that the generation of positive streamwise vorticity occurs behind the primary vortices ($P1$, $P2$), while the generation of negative streamwise vorticity occurs behind $S1$.

In this section, vorticity dynamics has been used to interpret the flow over a translating sphere. While analysis based on vortex visualisation methods alone, such as Gushchin & Matyushin (2006), provides a detailed qualitative description of the vortical structures in the wake, either vorticity or momentum considerations are required to understand their dynamical evolution. Lyman's definition of the vorticity flux allows key features of the flow to be understood by considering the fluxes of vorticity in the symmetry plane alone, providing a clear and elegant dynamical interpretation of the motion.

5. Conclusion

Vorticity dynamics provides a powerful framework for understanding the behaviour of various flows, and often provides a deeper understanding of flow behaviour than momentum considerations alone. While Lighthill's original definition of the boundary vorticity flux can provide insight into the generation and diffusion of vorticity, Lyman's alternative definition offers several compelling advantages. First, Lyman's definition more clearly demonstrates the kinematic relationship between vorticity and velocity: Lyman's
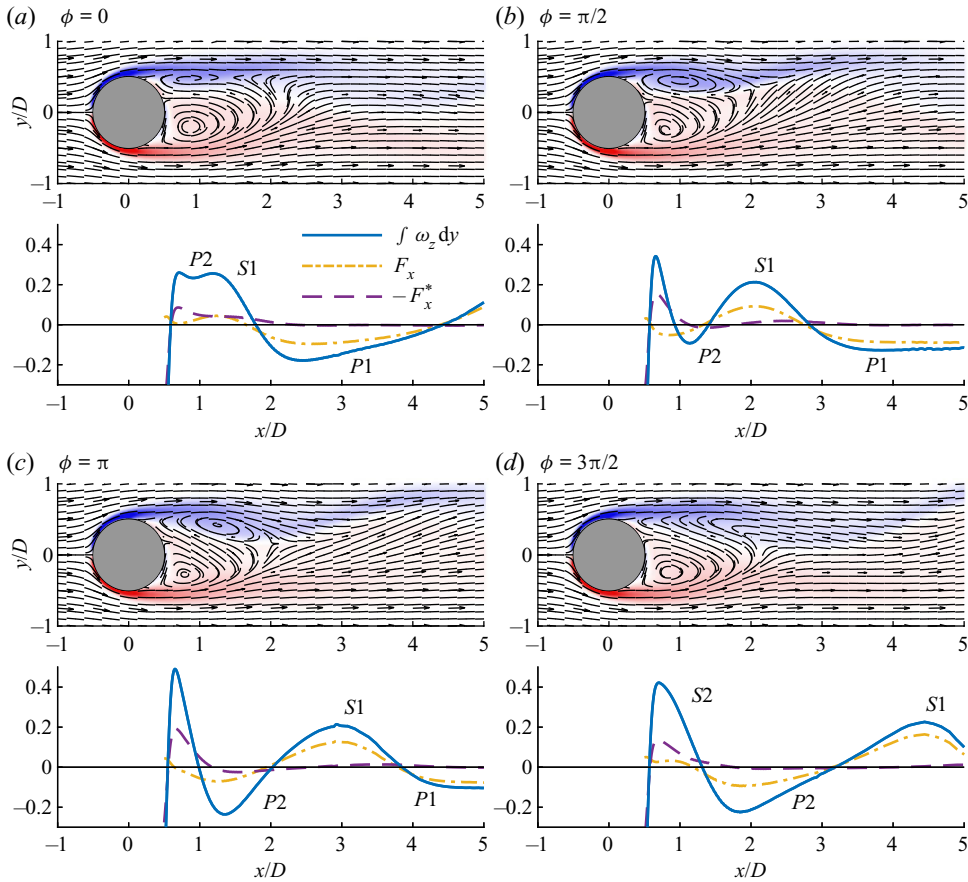
Figure 28. Colour contours of spanwise vorticity and velocity streamlines (top), and streamwise distributions of vorticity and vorticity fluxes in the symmetry plane (lower), over one period of vortex shedding. ϕ is the temporal phase angle, measured from the point of minimum lift coefficient (Johnson & Patel (1999) define ϕ from the point of maximum lift).
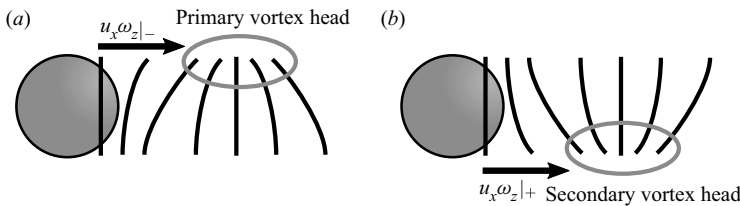

Figure 29. Schematic illustration of the generation of hairpin vortex structures. (*a*) Rapid shedding of negative vorticity from the upper wake produces the primary vortex head, as well as tilting vortex lines forwards, generating positive streamwise vorticity. (*b*) Rapid shedding of positive vorticity from the lower wake generates the secondary vortex head, and tilts vortex loops backwards, generating negative streamwise vorticity in the legs of this vortex.

flux is equal to the tangential viscous acceleration of boundary fluid elements, and this provides a direct link between the dynamics of vorticity and the dynamics of linear momentum.

Moreover, Lyman's definition also offers a simpler description of the generation of vorticity on a solid boundary, where the vorticity creation rate is determined by tangential pressure gradients, body forces and the acceleration of the solid boundary, and is independent of viscosity. This allows Morton's (1984) inviscid description of vorticity generation to be applied directly to three-dimensional flows, providing an intuitive conceptual model of the vorticity generation process.

Lyman's definition of the vorticity flux can also be related to the kinematic condition that vortex lines do not end inside the fluid. In vortex reconnection, Lyman's flux ensures that the loss of circulation from the symmetry plane is exactly balanced by the gain of circulation in the dividing plane, so that the cutting and reconnection of vortex lines are treated as a single process. Moreover, the generation of tangential vorticity on a rotating solid boundary is associated with the diffusion of normal vorticity along the surface, and this ensures that vortex lines do not end on the boundary. While Lighthill's definition can be used to describe these flows, it does not clearly illustrate how the kinematic condition on vortex lines is maintained.

Finally, Lyman's flux allows key features of the dynamics of three-dimensional flows to be understood by considering the fluxes of vorticity in an appropriate two-dimensional reference surface. Both the generation of streamwise vortical structures by vortex tilting and the viscous cross-annihilation of vorticity in the wake behind a sphere can be described and quantified by considering the fluxes of vorticity acting in the symmetry plane. The evolution of coherent vortical structures in the wake, identified by vortex visualisation techniques, cannot be understood without recourse to vorticity dynamics, and Lyman's definition of the vorticity flux provides an elegant interpretation of the dynamics of these structures.

Author ORCIDs.

Ⓓ S.J. Terrington https://orcid.org/0000-0001-9117-9170;

Ⓓ K. Hourigan https://orcid.org/0000-0002-8995-1851;

Ⓓ M.C. Thompson https://orcid.org/0000-0003-3473-2325.

Appendix A. Derivation of (2.2)

Consider the rate of change of circulation contained in an arbitrary reference surface,

$$\frac{\mathrm{d}\Gamma}{\mathrm{d}t} = \frac{\mathrm{d}}{\mathrm{d}t} \int_S \boldsymbol{\omega} \cdot \mathrm{d}\boldsymbol{S} = \frac{\mathrm{d}}{\mathrm{d}t} \oint_C \boldsymbol{u} \cdot \mathrm{d}\boldsymbol{s}, \tag{A1}$$

where C is the boundary curve of S, as illustrated in figure 1. By parametrising the boundary curve, $C = \boldsymbol{y}(s', t)$, the derivative may be taken inside the second integral,

$$\frac{\mathrm{d}}{\mathrm{d}t} \oint_C \boldsymbol{u} \cdot \mathrm{d}\boldsymbol{s} = \oint_C \left.\frac{\partial \boldsymbol{u}}{\partial t}\right|_{s'} \cdot \mathrm{d}\boldsymbol{s} + \oint_C \boldsymbol{u} \cdot \frac{\partial^2 \boldsymbol{y}}{\partial t \partial s'} \, \mathrm{d}s' = \oint_C \left.\frac{\partial \boldsymbol{u}}{\partial t}\right|_{s'} \cdot \mathrm{d}\boldsymbol{s} + \oint_C \boldsymbol{u} \cdot \frac{\partial \boldsymbol{v}^b}{\partial s} \, \mathrm{d}s, \tag{A2}$$

where $\boldsymbol{v}^b = \partial \boldsymbol{y}/\partial t$ is the velocity of the boundary curve. Using the momentum equation, the first term on the right-hand side of (A2) becomes

$$\oint_C \frac{\partial \boldsymbol{u}}{\partial t}\bigg|_{s'} \cdot \mathrm{d}\boldsymbol{s} = \oint_C \left[(\boldsymbol{v}^b - \boldsymbol{u}) \cdot \boldsymbol{\nabla}\boldsymbol{u} \right] \cdot \mathrm{d}\boldsymbol{s} + \oint_C [-\nu \boldsymbol{\nabla} \times \boldsymbol{\omega}] \cdot \mathrm{d}\boldsymbol{s}, \tag{A3}$$

since the partial derivative is with respect to a moving frame. The advection term can be replaced by the Lamb vector,

$$\oint_C [\boldsymbol{u} \cdot \boldsymbol{\nabla}\boldsymbol{u}] \cdot \mathrm{d}\boldsymbol{s} = \oint_C (\boldsymbol{\omega} \times \boldsymbol{u}) \cdot \mathrm{d}\boldsymbol{s}, \tag{A4}$$

while the remaining terms containing $\boldsymbol{v}^b$ in (A2) and (A3) can be simplified:

$$\oint_C \left[\boldsymbol{v}^b \cdot \boldsymbol{\nabla}\boldsymbol{u} \cdot \hat{\boldsymbol{t}} + \hat{\boldsymbol{t}} \cdot \boldsymbol{\nabla}\boldsymbol{v}^b \cdot \boldsymbol{u} \right] \mathrm{d}s = \oint_C \left[\boldsymbol{v}^b \cdot \boldsymbol{\nabla}\boldsymbol{u} + (\boldsymbol{\nabla}\boldsymbol{v}^b) \cdot \boldsymbol{u} \right] \cdot \mathrm{d}\boldsymbol{s}. \tag{A5}$$

After using the product rule on the final term, we obtain the following expression:

$$\oint_C \left[\boldsymbol{v}^b \cdot \boldsymbol{\nabla}\boldsymbol{u} + (\boldsymbol{\nabla}\boldsymbol{v}^b) \cdot \boldsymbol{u} \right] \cdot \mathrm{d}\boldsymbol{s} = \oint_C \left[\boldsymbol{v}^b \cdot \boldsymbol{\nabla}\boldsymbol{u} - (\boldsymbol{\nabla}\boldsymbol{u}) \cdot \boldsymbol{v}^b \right] \cdot \mathrm{d}\boldsymbol{s} = \oint_C (\boldsymbol{\omega} \times \boldsymbol{v}^b) \cdot \mathrm{d}\boldsymbol{s}. \tag{A6}$$

Finally, on substituting these results into (A1), we obtain

$$\frac{\mathrm{d}\Gamma}{\mathrm{d}t} = \oint_C \left[\boldsymbol{\omega} \times (\boldsymbol{v}^b - \boldsymbol{u}) - \nu \boldsymbol{\nabla} \times \boldsymbol{\omega} \right] \cdot \mathrm{d}\boldsymbol{s}, \tag{A7}$$

and by using a vector identity, Lyman's flux appears in this expression:

$$\frac{\mathrm{d}\Gamma}{\mathrm{d}t} = \oint_C \left[\hat{\boldsymbol{n}} \times \left[(\boldsymbol{u} - \boldsymbol{v}^b) \times \boldsymbol{\omega} - \nu(\boldsymbol{\nabla} \times \boldsymbol{\omega}) \right] \right] \cdot \hat{\boldsymbol{s}} \, \mathrm{d}s. \tag{A8}$$

REFERENCES

BEARDSELL, G., DUFRESNE, L. & DUMAS, G. 2016 Investigation of the viscous reconnection phenomenon of two vortex tubes through spectral simulations. *Phys. Fluids* **28** (9), 095103.

BERNARD, P.S. 2011 The hairpin vortex illusion. *J. Phys.: Conf. Ser.* **318**, 062004.

BERNARD, P.S. 2019 On the inherent bias of swirling strength in defining vortical structure. *Phys. Fluids* **31** (3), 035107.

BRØNS, M., THOMPSON, M.C., LEWEKE, T. & HOURIGAN, K. 2014 Vorticity generation and conservation for two-dimensional interfaces and boundaries. *J. Fluid Mech.* **758**, 63–93.

CALABRETTO, S.A.W., DENIER, J.P & LEVY, B. 2019 An experimental and computational study of the post-collisional flow induced by an impulsively rotated sphere. *J. Fluid Mech.* **881**, 772–793.

CALABRETTO, S.A.W., LEVY, B., DENIER, J.P. & MATTNER, T.W. 2015 The unsteady flow due to an impulsively rotated sphere. *Proc. R. Soc.* A **471**, 20150299.

CHORIN, A.J. 1973 Numerical study of slightly viscous flow. *J. Fluid Mech.* **57** (4), 785–796.

EYINK, G.L. 2008 Turbulent flow in pipes and channels as cross-stream "inverse cascades" of vorticity. *Phys. Fluids* **20** (12), 125101.

EYINK, G.L., GUPTA, A. & ZAKI, T.A. 2020 Stochastic Lagrangian dynamics of vorticity. Part 1. General theory for viscous, incompressible fluids. *J. Fluid Mech.* **901**, A2.

FUENTES, O.U.V. 2007 On the topology of vortex lines and tubes. *J. Fluid Mech.* **584**, 147–156.

GREENE, J.M. 1993 Reconnection of vorticity lines and magnetic lines. *Phys. Fluids* B **5** (7), 2355–2362.

GRESHO, P.M. 1991 Incompressible fluid dynamics: some fundamental formulation issues. *Annu. Rev. Fluid Mech.* **23** (1), 413–453.

GUSHCHIN, V.A., KOSTOMAROV, A.V., MATYUSHIN, P.V. & PAVLYUKOVA, E.R. 2002 Direct numerical simulation of the transitional separated fluid flows around a sphere and a circular cylinder. *J. Wind Engng Ind. Aerodyn.* **90** (4–5), 341–358.

GUSHCHIN, V.A. & MATYUSHIN, R.V. 2006 Vortex formation mechanisms in the wake behind a sphere for $200 < Re < 380$. *Fluid Dyn.* **41** (5), 795–809.

HUGGINS, E.R. 1971 Dynamical theory and probability interpretation of the vorticity field. *Phys. Rev. Lett.* **26** (21), 1291–1294.

HUGGINS, E.R. 1994 Vortex currents in turbulent superfluid and classical fluid channel flow, the Magnus effect, and Goldstone boson fields. *J. Low Temp. Phys.* **96** (5–6), 317–346.

HUGGINS, E.R. & BACON, D.P. 1980 Vortex currents and hydrodynamic instability in Taylor cells. *Phys. Rev.* A **21** (4), 1327–1330.

JEONG, J. & HUSSAIN, F. 1995 On the identification of a vortex. *J. Fluid Mech.* **285**, 69–94.

JOHNSON, T.A. & PATEL, V.C. 1999 Flow past a sphere up to a Reynolds number of 300. *J. Fluid Mech.* **378**, 19–70.

KIDA, S. & TAKAOKA, M. 1991 Breakdown of frozen motion of vorticity field and vorticity reconnection. *J. Phys. Soc. Japan* **60** (7), 2184–2196.

KIDA, S. & TAKAOKA, M. 1994 Vortex reconnection. *Annu. Rev. Fluid Mech.* **26** (1), 169–177.

KOLÁR, V. 2003 On the Lyman problem. *Cent. Eur. J. Phys.* **1** (2), 258–267.

KÜCHEMANN, D. 1965 Report on the I.U.T.A.M. symposium on concentrated vortex motions in fluids. *J. Fluid Mech.* **21**, 1–20.

KUSTEPELI, A. 2016 On the Helmholtz theorem and its generalization for multi-layers. *Electromagnetics* **36** (3), 135–148.

LEONARD, A. 1980 Vortex methods for flow simulation. *J. Comput. Phys.* **37** (3), 289–335.

LIGHTHILL, M.J. 1963 Introduction: boundary layer theory. In *Laminar Boundary Layers* (ed. L. Rosenhead), chap. 2, pp. 46–109. Oxford University Press.

LYMAN, F.A. 1990 Vorticity production at a solid boundary. *Appl. Mech. Rev.* **43** (8), 157–158.

MCGAVIN, P. & PONTIN, D.I. 2018 Vortex line topology during vortex tube reconnection. *Phys. Rev. Fluids* **3** (5), 054701.

MELANDER, M.V. & HUSSAIN, F. 1989 Cross-linking of two antiparallel vortex tubes. *Phys. Fluids* A **1** (4), 633–636.

MELANDER, M.V. & HUSSAIN, F. 1990 Topological aspects of vortex reconnection. In *Topological Fluid Mechanics* (ed. H.K. Moffatt & A. Tsinober), pp. 485–499. Cambridge University Press.

MORINO, L. 1986 Helmholtz decomposition revisited: vorticity generation and trailing edge condition. *Comput. Mech.* **1** (1), 65–90.

MORTON, B.R. 1984 The generation and decay of vorticity. *Geophys. Astrophys. Fluid Dyn.* **28**, 277–308.

PANTON, R.L. 1984 *Incompressible Flow*. John Wiley and Sons.

PAYNE, R.B. 1956 A numerical method for calculating the starting, and perturbation of a two-dimensional jet at low Reynolds number. *Tech. Rep.* 3047. Aero. Res. Counc. (Lond.), Rep. & Mem.

PAYNE, R.B. 1958 Calculations of unsteady viscous flow past a circular cylinder. *J. Fluid Mech.* **4** (1), 81–86.

SAFFMAN, P.G. 1990 A model of vortex reconnection. *J. Fluid Mech.* **212**, 395–402.

STANAWAY, S., SHARIFF, K. & HUSSAIN, F. 1988 Head-on collision of viscous vortex rings. In *Studying Turbulence Using Numerical Simulation Databases 2: Proceedings of the 1988 CTR Summer Program*, pp. 257–286. Stanford University.

TAKAOKA, M. 1996 Helicity generation and vorticity dynamics in helically symmetric flow. *J. Fluid Mech.* **319**, 125–149.

TERRINGTON, S.J., HOURIGAN, K. & THOMPSON, M.C. 2020 The generation and conservation of vorticity: deforming interfaces and boundaries in two-dimensional flows. *J. Fluid Mech.* **890**, A5.

THOMPSON, M.C., LEWEKE, T. & PROVANSAL, M. 2001 Kinematics and dynamics of sphere wake transition. *J. Fluids Struct.* **15** (3–4), 575–585.

TIWARI, S.S., PAL, E., BALE, S., MINOCHA, N., PATWARDHAN, A.W., NANDAKUMAR, K. & JOSHI, J.B. 2020 Flow past a single stationary sphere, 2. Regime mapping and effect of external disturbances. *Powder Technol.* **365**, 215–243.

TRUESDELL, C. 1954 *The Kinematics of Vorticity*. Indiana University Press.

WU, J.Z. 1995 A theory of three-dimensional interfacial vorticity dynamics. *Phys. Fluids* **7** (10), 2375–2395.

WU, J.Z. & WU, J.M. 1993 Interactions between a solid surface and a viscous compressible flow field. *J. Fluid Mech.* **254**, 183–211.

WU, J.Z. & WU, J.M. 1996 Vorticity dynamics on boundaries. *Adv. Appl. Mech.* **32**, 119–275.

WU, J.Z. & WU, J.M. 1998 Boundary vorticity dynamics since Lighthill's 1963 article: review and development. *J. Theor. Comput. Fluid Dyn.* **10** (1–4), 459–474.